

Few-Shot Hyperspectral Image Classification With Unknown Classes Using Multitask Deep Learning

Shengjie Liu, *Member, IEEE*, Qian Shi, *Senior Member, IEEE*, and Liangpei Zhang, *Fellow, IEEE*

Abstract—Current hyperspectral image classification assumes that a predefined classification system is closed and complete, and there are no unknown or novel classes in the unseen data. However, this assumption may be too strict for the real world. Often, novel classes are overlooked when the classification system is constructed. The closed nature forces a model to assign a label given a new sample and may lead to overestimation of known land covers (e.g., crop area). To tackle this issue, we propose a multitask deep learning method that simultaneously conducts classification and reconstruction in the open world (named MDL4OW) where unknown classes may exist. The reconstructed data are compared with the original data; those failing to be reconstructed are considered unknown, based on the assumption that they are not well represented in the latent features due to the lack of labels. A threshold needs to be defined to separate the unknown and known classes; we propose two strategies based on the extreme value theory for few-shot and many-shot scenarios. The proposed method was tested on real-world hyperspectral images; state-of-the-art results were achieved, e.g., improving the overall accuracy by 4.94% for the Salinas data. By considering the existence of unknown classes in the open world, our method achieved more accurate hyperspectral image classification, especially under the few-shot context.

Index Terms—multitask learning, deep learning, convolutional neural network, hyperspectral image classification, open-set recognition, classification with unknown classes

I. INTRODUCTION

The world's urbanization has rapidly developed since the 1980s. With the growing population, the large number of human beings living on this small planet becomes a crucial problem. Sufficient food supplies are needed to feed human beings, but sufficient land resources for daily life activities are also needed [1]. Ongoing urbanization transforms natural environments into cities and increases the fraction of the impervious surface, eliminating rainwater infiltration and increasing the urban temperature. Planning land resource usage

This is the preprint version. To read the final version please go to <https://doi.org/10.1109/TGRS.2020.3018879>

Manuscript received May 11, 2020; accepted August 18, 2020. This work was supported in part by the National Natural Science Foundation of China under Grant 61976234, and in part by Guangdong Basic and Applied Basic Research Foundation under Grant 2019A1515011057. (*Corresponding author: Qian Shi.*)

Shengjie Liu is with the Department of Physics, The University of Hong Kong, Pokfulam, Hong Kong (e-mail: sjliu.me@gmail.com).

Qian Shi is with the Guangdong Provincial Key Laboratory of Urbanization and Geo-simulation, School of Geography and Planning, Sun Yat-sen University, Guangzhou 510275, China (e-mail: shixi5@mail.sysu.edu.cn).

Liangpei Zhang is with the State Key Laboratory of Information Engineering in Surveying, Mapping and Remote Sensing and the Collaborative Innovation Center of Geospatial Technology, Wuhan University, Wuhan 430079, China (e-mail: zlp62@whu.edu.cn).

wisely is the key to maintaining the world's sustainability, and this requires timely and accurate land cover monitoring.

Existing methods for land cover mapping include land survey and classification based on satellite and airborne remote sensing images. A land survey is impractical for large area monitoring as it is labor-intensive and time-consuming. Classifying each pixel of a satellite image is a more popular way. Two existing semi-automatic methods can be applied, i.e., semantic segmentation and pixel-wise classification. Semantic segmentation considers the entire image as a sample instance and directly outputs the segmentation result [2]; it requires a large set of fully annotated images [3]. This approach is not practical for detailed land cover mapping, as a) the land cover classification system is very complex, and b) the satellite data are quite diverse. Specifically, depending on the application, a remote sensing image can be either mapped into 3-4 classes (impervious, vegetation, water, and sometimes barren) or 10+ fine-grained classes [4]–[6]. The land cover classification system is multilevel. On the other hand, the sources of remote sensing images are diverse, making it difficult to reuse previous datasets. For optical remote sensing, the number of spectral bands ranges from one to hundreds. The diversity increases if non-optical data (e.g., PolSAR) are included. As a result, pixel-wise classification is more popular for land cover mapping.

Remotely sensed hyperspectral images, due to their rich spectral information, are of great use for land cover classification. The physical theory for hyperspectral image classification is that each class can be separated based on its spectral profiles. Due to its great potential, hyperspectral image classification has gone through rapid development in the last two decades [7]–[9]. In the early 2000s, hyperspectral images were solely considered as sequential data, as shown in the classic 2-D storage format (#sample × #feature). At this stage, support vector machines (SVMs) were the mainstream classifiers [10]–[12]. SVMs with kernels can project hyperspectral data to a high-dimensional hyperplane, where the training data should be highly separated based on their class belongings. In the late 2000s, with the popularity of graph models (e.g., Markov random fields [13]), morphological profiles [14], and other spatial filters, including edge-preserving filters and Gabor filters [15], [16], spectral-spatial classification of hyperspectral data became a popular topic and influenced the last ten years [7]. At the same time, many advanced algorithms tackling the limited availability of training samples were proposed, including active learning [17], [18], semi-supervised learning [19], [20], graph models [21], sparse representation [22], [23], and domain adaptation [24]. Since the classification

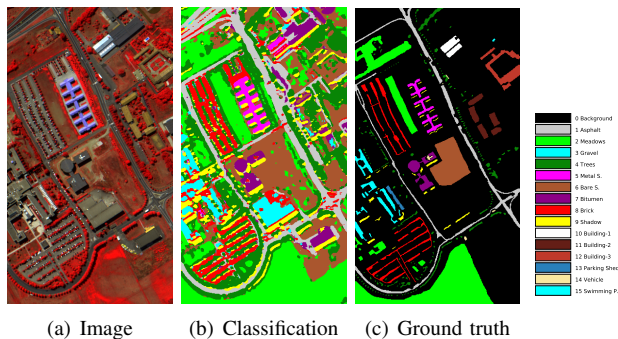


Fig. 1. Example of the University of Pavia’s classification map (nine classes, OA=98%). The original ground truth covers only nine classes. We manually annotated six additional classes, which were unknown to the classifier. Note building-1, building-2 and building-3 on the right are misclassified as a mix of bare soil and other materials. The swimming pool, helicopters (vehicle) and the parking shed are all misclassified as natural land covers.

performance also depends on the dimension due to the curse of dimensionality, band selection and dimension reduction techniques are widely used in hyperspectral image classification [25]–[27].

In the deep learning era, the novel convolutional neural networks (CNNs), recurrent neural networks and graph convolutional networks started to dominate the classification of hyperspectral and remote sensing data [9], [28]–[34]. Manual feature engineering was replaced by automatic feature learning by deep networks. Now, hyperspectral image classification entered the stage with 99% classification accuracy with sufficient training samples [35]. Besides, many works have focused on improving the few-shot classification accuracy (classification with limited samples), including deep few-shot learning (DFSL) with neural networks and SVM [36], spatial-spectral relation network (SS-RN) [37], and deep relation network [38]. However, the high accuracy is achieved under the assumption that there is no unknown class in the unseen data. If an instance does not belong to any of the known classes, this instance will not harm the classification accuracy from the current evaluation system, as such instance will not be considered. But the existence of unknown or novel classes will lead to false positives and thereby reduce the precision of a model. If many instances belong to the unknown class are classified as a known class, the number of the known classes will be largely overestimated. Unfortunately, in the real world, it is difficult, if not impossible, to define all potential classes. As mentioned, a sample collection based on a field survey can only cover a small portion of the study area due to budget limits. For example, [39] collected ground truth data along the major road network, and those buried far from the road network were inevitably neglected. Therefore, a machine learning model trained on the collected samples might face some instances (the unknown) that cannot be classified into one of the known classes.

The influence of unknown classes, although dependent on the area of an image, may even occur in a very small study region. The University of Pavia dataset, one of the most popular hyperspectral benchmarks, records nine land cover classes in a region of 610×340 with $1.3 m$ ground sampling

distance (GSD), approximately $793 \times 442 m^2$. This dataset is small and barely covers a campus. However, there is a swimming pool that should not belong to any of the nine classes. We show the false color map of the University of Pavia data in Figure 1, where the swimming pool is located on the upper right side of the image. In addition, on the right side of the image, three groups of buildings (building-1, building-2, building-3) are not annotated in the original reference map. These buildings are often misclassified as natural land covers such as bare soil [35], [40]–[42] and meadows [43], or other unrelated materials such as asphalt [44], [45].

The assumption that all test data are known in machine learning is called a closed world or closed set [46], [47]. In the closed world, given an unknown instance that cannot be classified as one of the known classes, a model will eventually assign a known class label to the unknown instance because it cannot identify it as unknown. In this case, if the model is used to map certain crop types, it is inevitable to overestimate their area and, therefore, the total amount of food supplies.

The closed-world setting is not enough for accurate hyperspectral image classification. The machine needs to tell the unknown from known classes. This is impossible for many algorithms, as they assume a closed-world setting. For example, the deep neural network is limited by the SoftMax function, which constrains the output probabilities to have a summation of one, and each is within zero to one. In this scenario, one of the known classes must be assigned for the input instance. A simple solution is using confidence thresholding, rejecting those with low classification confidence. However, low classification confidence is not the assurance of the unknown; instead, it is uncertain [46]. An uncertain instance may be a valuable sample close to the classification hyperplane’s boundary for active learning, instead of the unknown [48].

To tackle the open world problem, some methods were proposed for daily image recognition. First named as open-set recognition by [46], they introduced 1-vs-set machine to empower SVM with the capability to identify the unknown. The OpenMax method is the first one tackling this problem under the context of deep learning [49], which enables the network to estimate the probability of one instance being the unknown class. It used the activation vectors (the final layer’s output features before SoftMax) to estimate the distance distribution of each class and then applied the extreme value theory to recalibrate the activation vector with $C+1$ classes, where the added class was the unknown. [50] proposed to use counterfactual images generated from generative adversarial networks as the unknown to train the classifier. Furthermore, [51] argued to use the background classes to reduce the network agnostophobia. Further, [52] added an auxiliary task to enhance the latent features for the OpenMax method. This enhanced method for open-set recognition, named CROSR, was tested with anomaly detection algorithms, i.e., IsoForest and one-class SVM, in a class-wise fashion, to exploit the latent features effectively. The method achieved the current state of the art in open-set recognition. However, like other methods, a large amount of training samples were still needed to estimate the centroid of each class, limiting its performance in hyperspectral image classification.

The above-mentioned methods for daily image recognition are mostly centroid-based, where the unknown score is calculated in a class-wise fashion, which limits their usage under the few-shot context. For example, the CIFAR dataset consists of 600 samples per class [53], and the fashion-MNIST consists of 7000 samples per class [54]. In hyperspectral image classification, the size of the training set is significantly smaller than the daily image recognition as collecting ground truth data is labor-intensive and time-consuming. Sometimes, only 5 to 20 instances per class are available for training [36], [55], [56], limiting the usage of these open-set methods for hyperspectral image classification. Another difference between daily image recognition and hyperspectral image classification is that the number of potential classes is smaller in the latter, as hyperspectral images are taken from the same direction (overhead), whereas daily images are more complex. For hyperspectral images, it is rare to have more than 20 classes in a dataset; but, for daily image recognition, the number of classes already exceeds one thousand, e.g., ImageNet [57]. As a direct result of fewer potential classes, the openness (unknown degree) of hyperspectral image classification is significantly smaller than daily image recognition. Often, the unknown or novel instances count for only a small portion of the study area, which is called the tail class in technical terms, e.g., swimming pools and vehicles. The low openness significantly affects the performance of current open-set techniques as they are designed to face a larger open world [58]. In summary (as shown in Table I), due to the three notable differences between hyperspectral image classification and daily image open-set recognition (few-shot, fewer classes, and low openness), it is difficult to directly use open-set techniques developed for daily image recognition in hyperspectral image classification.

In this paper, tackling the few-shot nature, we propose a novel multitask deep learning method for hyperspectral image classification with unknown classes in the open world (MDL4OW), which is free from estimating the class centroid in a class-wise fashion. The proposed method utilizes multitask learning to conduct classification and reconstruction simultaneously. The unknown score is calculated by comparing the original and reconstructed data, whereas the unknown should be poorly reconstructed due to the lack of labels. In this way, the proposed MDL4OW does not need to calculate the mean activation vectors or latent features in a class-wise fashion. Therefore, it is suitable for few-shot hyperspectral image classification. The major contributions of this study are summarized as follows:

- We propose a novel multitask deep learning method named MDL4OW for hyperspectral image classification with unknown classes. The proposed method can identify unknown classes and significantly improve the classification accuracy.
- Instead of estimating the unknown score in a class-wise manner using centroid-based methods, the proposed method can estimate the unknown score with all data using the statistical model extreme value theory. Therefore, the proposed method outperformed the state-of-the-art open-set technique for few-shot hyperspectral image

classification.

- A new evaluation metric, the mapping error, is proposed to evaluate the accuracy of hyperspectral image classification with unknown classes. This metric is especially sensitive to imbalanced classification, which is often the case in hyperspectral images.

The remainder of this paper is organized as follows. In the next section, we describe the methodology in detail. In section III, we introduce the evaluation metrics and the experimental setup. In section IV, we discuss the experimental results obtained on real-world datasets and provide analyses. Finally, we present our conclusions in section V.

II. METHODOLOGY

In this section, we review a single-task classification network's components, including a feature extractor (encoder) and a classifier. Then, we describe the proposed multitask network in detail, including an encoder-decoder structure which is used to reconstruct the input instance. Based on the assumption that instances with labels from the classification system can be better reconstructed than the unknown, those with a large reconstructed loss should be rejected and considered as unknown. Finally, extreme value theory is used to separate the unknown from known classes.

A. Deep CNNs for classification

The proposed network with the flowchart is shown in Figure 2, which consists of two residual learning blocks [59] and a global average pooling layer [60] as the encoder, a fully connected layer with the SoftMax function as the classifier, and a decoder with deconvolutional layers [61]. The classification part is a modified version of HResNet [43] when adding the global average pooling layer.

The powerful ability of deep CNNs for hyperspectral image classification tasks lies in the usage of convolutional layers to extract spectral-spatial information [62]. Considering X as the sample instance space, where each instance $x \in X$, given a limited training set with index k consisting of only a few samples (x^k, l^k) , where $l^k \in L = \{1, \dots, |C|\}$ is the label index for x^k , the multilevel convolutional layers, along with batch normalization [63], and the rectified linear unit (ReLU) [64], serve as a good encoder $\phi(\cdot)$ to extract the spectral-spatial features x_ϕ as the representation of the sample instance:

$$x_\phi = \phi(x). \quad (1)$$

In the encoder, the output of a convolutional layer $\phi_{conv}(\cdot)$ can be simplified as

$$x_{\phi_{conv}} = \phi_{conv}(x). \quad (2)$$

Then, the classifier $f(\cdot)$ takes the output vector x_ϕ from the feature extractor $\phi(\cdot)$ as its input. In a pure deep learning scenario, the fully connected layer with the SoftMax activation function serves as the classifier $f(\cdot)$ and gives the probability $P(y = j|x_\phi)$ of the j -th category:

$$P(y = j|x_\phi) = \frac{\exp(x_\phi^T w_j + b_j)}{\sum_{c=1}^C \exp(x_\phi^T w_c + b_c)}, \quad (3)$$

TABLE I
COMPARISON AMONG HYPERSPECTRAL IMAGE CLASSIFICATION WITH UNKNOWN CLASSES AND THE EXISTING TASKS.

Task	Few-shot	Unknown classes	Openness	#Class	#Channel
Daily photo recognition	Rare (often >500)	Yes	High	100+	1-4
Hyperspectral image classification	Often (<50)	No	0	20-	Up to 300+
Hyperspectral image classification with unknown classes	Often (<50)	Yes	Low	20-	Up to 300+

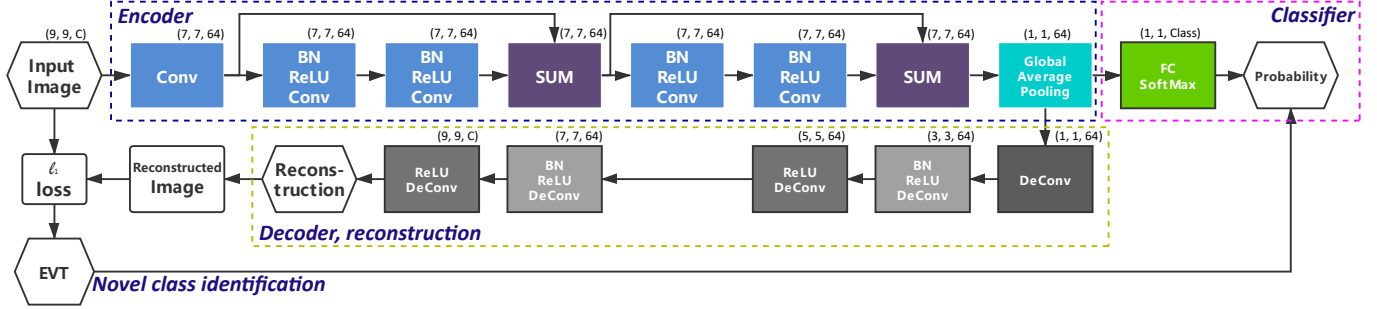


Fig. 2. Flowchart of the proposed method. The multitask network used here takes an input of $9 \times 9 \times \text{Channel}$. The first part of the network is an encoder/feature extractor with two residual units and a global average pooling layer. After extracting the latent features, a fully connected layer with the softmax function serves as the classifier and outputs the probability to the known classes. The reconstruction task here uses the deconvolutional layers to increase the spatial dimension of the latent features gradually. The output of the reconstruction task is a $9 \times 9 \times \text{Channel}$ instance, which should be similar to the input data by minimizing the ℓ_1 loss. The reconstruction loss is modeled by EVT to separate the known and unknown classes.

where w_j is the weight vector of the j -th neuron in the fully connected layer, b_j is a bias element corresponding to the j -th neural, and C is the number of the category. The classification task is to find the optimal parameters for the network by minimizing the cross-entropy loss function ℓ_c :

$$\ell_c(y, \hat{y}) = - \sum_{i=1}^C y_i \log(\hat{y}_i), \quad (4)$$

where C is the number of predefined classes, y is the ground truth label, and \hat{y} is the predicted label.

As mentioned, the SoftMax function transforms the score vector into a probability vector, and the class with the largest probability is considered the predicted class. A naive solution to identify unknown classes is considering those instances with the largest probability smaller than 0.5 as unknown, which is one of the baselines in the experiments (SoftMax with threshold = 0.5).

B. Reconstruction via multitask learning

So far, the feature extractor and classifier together form a decent machine for classification, but the network cannot still identify the unknown. To empower the network with this ability, we add a reconstruction task:

$$\hat{x} = f_r(x_\phi), \quad (5)$$

where \hat{x} is the reconstructed instance, $f_r(\cdot)$ is the reconstruction function or named the decoder, and x_ϕ is the output latent features from the encoder $\phi(\cdot)$. Here, we use ℓ_1 distance as the reconstruction loss,

$$\ell_r(x, \hat{x}) = \|x - \hat{x}\|_1. \quad (6)$$

In the training phase for the multitask network, we minimize the total loss via backpropagation,

$$\min_{\phi(\cdot), f_c(\cdot), f_r(\cdot)} \lambda_c \ell_c(y, \hat{y}) + \lambda_r \ell_r(x, \hat{x}), \quad (7)$$

where λ_c and λ_r are the weights to control the loss influence on the multitask network for ℓ_c and ℓ_r , respectively.

In the decoder, the key element is the deconvolutional layer, also called the transposed convolutional layer. It can be considered as the inverse of a convolutional layer, denoted as $\phi_{conv}^\dagger(\cdot)$, resulting:

$$x = \phi_{conv}^\dagger(\phi_{conv}(x)). \quad (8)$$

Using the deconvolutional layer, we can gradually increase the $1 \times 1 \times \text{channel}$ latent features to patch-based hyperspectral sample instances. As shown in the flowchart (Figure 2), the reconstruction branch of the proposed method consists of a total of five deconvolutional layers, where all increase the spatial dimension of the instance except for the first one.

C. Threshold setting with extreme value theory

After obtaining the reconstruction losses (an example is shown in Figure 3), where a larger loss indicates that the deep learning model is not sufficiently optimized for the instance; the tail part of the loss distribution should be considered as unknown to the model. Here, we adopt the extreme value theory (EVT) to find the unknown classes by modeling a distribution of the tail part.

The EVT suggests that the tail should be a Weibull distribution [65]. For a large class of distributions, V , and a large enough threshold, w , with $\{V_1, \dots, V_n\}$, n independent and identically distributed samples, the cumulative distribution

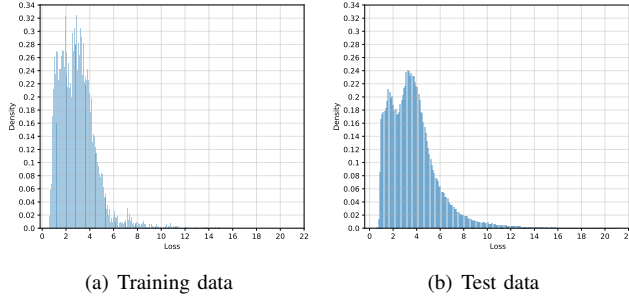


Fig. 3. Histogram samples of the reconstruction loss.

function can be approximated by a generalized pareto distribution (GPD):

$$P(v - w \leq v | v > w) = \frac{F_V(w + v) - F_V(w)}{1 - F_V(w)} \quad (9)$$

$$= G_{\xi, \mu}(v) \quad (10)$$

where,

$$G_{\xi, \mu}(v) = \begin{cases} 1 - \left(1 + \frac{\xi \cdot v}{\mu}\right)^{-\frac{1}{\xi}} & \xi \neq 0 \\ 1 - e^{-\frac{v}{\mu}} & \xi = 0 \end{cases} \quad (11)$$

where $\mu > 0$, and $v \geq 0$ when $\xi \geq 0$, and $0 \leq v \leq -\frac{\mu}{\xi}$ when $\xi < 0$. The parameters ξ and μ can be estimated from the given tail data [66]. Here, v is the reconstruction loss, and $G_{\xi, \mu}(\cdot)$ is the cumulative distribution function of GPD. The pseudocode for identifying the unknown class after obtaining the trained network is shown in Algorithm 1.

To model the tail distribution, one defines the tail size, τ , and a threshold value, z , to decide the boundary score between known and novel. The threshold is often set as 0.5 [49], [52], whereas the τ value should be at least two to model a distribution. The proposed method MDL4OW is free from class centroid estimation, which enhances its performance under the few-shot context. For comparison purposes, the class-wise version MDL4OW/C is also applied. The two methods are similar, except that MDL4OW is applied in a global fashion and MDL4OW/C is applied a class-wise fashion. Details of the threshold setting in the experiments are shown in section III-C experimental setup.

III. DATASETS AND EXPERIMENTAL SETUP

A. Datasets

1) *University of Pavia*: The first dataset used in the experiment is the previously mentioned benchmark, the University of Pavia. This image was captured by the ROSIS sensor over the University of Pavia campus in 2001. After removal of 12 bands affected by noise and water absorption, it contains 103 bands with a scene size of 610×340 in a GSD of 1.3 m. The standard reference map contains nine classes. As mentioned in the introduction section, some of the unannotated buildings have a very different spectral profile as compared to the known land covers. We manually annotated six additional classes, as shown in the reference map in Figure 4. The number of supporting reference pixels is available in Table II.

Algorithm 1 MDL4OW

Input: $X, \phi(\cdot), f(\cdot), f_r(\cdot), G_{\xi, \mu}(v), \tau, z$
Output: y_{pred}

- 1: Latent features: $X_\phi = \phi(X)$
- 2: Predicted known class: $y_{pred} = f(X_\phi)$
- 3: Reconstruction: $\hat{X} = f_r(X_\phi)$
- 4: Reconstruction error: $v = \|X - \hat{X}\|_1$
- 5: Compute EVT model $G_{\xi, \mu}(v)$ based on v, τ
- 6: **if** $G_{\xi, \mu}(v) < z$ **then**
- 7: $y_{pred} = y_{pred}$
- 8: **else**
- 9: $y_{pred} = unknown$
- 10: **end if**
- 11: **return** y_{pred}

TABLE II
THE UNIVERSITY OF PAVIA

Index	Name	#sample
1	Asphalt	6631
2	Meadows	18649
3	Gravel	2099
4	Trees	3064
5	Metal sheet	1345
6	Bare soil	5029
7	Bitumen	1330
8	Brick	3682
9	Shadow	947
	Novel	5163
Total		47939

TABLE III
SALINAS VALLEY

Index	Name	#sample
1	Weeds-1	2009
2	Weeds-2	3726
3	Fallow	1976
4	Fallow-P	1394
5	Fallow-S	2678
6	Stubble	3959
7	Celery	3579
8	Grapes	11271
9	Soil	6203
10	Corn	3278
11	Lettuce-4wk	1068
12	Lettuce-5wk	1927
13	Lettuce-6wk	916
14	Lettuce-7wk	1070
15	Vinyard-U	7268
16	Vinyard-T	1807
	Novel	5613
Total		59742

2) *Salinas Valley*: The Salinas Valley dataset was used in the experiment to evaluate the proposed method in fine-grained crop mapping using hyperspectral data. This image was collected by the AVIRIS sensor over Salinas Valley, California, with a GSD of 3.7 m. The region covers an area of 512×217 pixels with 204 bands after 20 water absorption bands were discarded. The data were at-sensor radiance data

TABLE IV
INDIAN PINES

Index	Name	#sample
1	Corn-notill	1428
2	Corn-mintill	830
3	Grass-pasture	483
4	Hay-windrowed	478
5	Soybean-notill	972
6	Soybean-mintill	2454
7	Soybean-clean	593
8	Woods	1265
	Novel	2007
Total		10510

without atmospheric correction. A total of 16 agricultural land covers are identified in the image. However, some of the man-made materials, such as buildings, are not represented in the classification system and should not be classified as any of the known crops. We manually annotated these man-made materials and a water pool as the unknown, as shown in Figure 5 reference map. Details of the dataset can be found in Table III.

3) *Indian Pines*: The Indian Pines dataset is used to illustrate the potential of the proposed method. The dataset was captured by the AVIRIS sensor in 1992 over the Indian Pines test site in Northwest Tippecanoe County, Indiana. The image consists of 145×145 pixels with a GSD of 20 m. A total of 16 classes were annotated in the reference data, and most were agricultural land covers. A road exists on the upper side of the image, which should not belong to any of the known classes. We manually annotated the road, as shown in Figure 6 reference map. Since some of the classes only have less than ten instances, these tail classes were discarded in the experiment following [29] and were considered as unknown, resulting in eight known classes. Details of the dataset can be found in Table IV.

B. Evaluation metrics

1) *Openness*: Openness indicates the unknown or open degree of a dataset for open-world classification. It can be calculated from the number of training classes and the number of test classes [68]:

$$Openness = 1 - \sqrt{\frac{2 \times N_{train}}{N_{test} + N_{train}}}. \quad (12)$$

Low openness is one of the differences between daily image recognition and hyperspectral image classification. Some studies pointed out that the performance of certain methods could be degraded with a low openness value [58]. The openness values for the three hyperspectral datasets are 13%, 3%, and 20%, whereas the openness for daily image recognition is up to 63% [67].

2) *Open overall accuracy (OA)*: The evaluation of open-world classification is critical and diverse because of the inclusion of unknown classes [68]. A naive solution is extending

the current OA evaluation metric from C classes to $C + 1$ classes, where the added is the unknown class.

$$Open\ OA = \frac{\sum_{i=1}^{C+1} (TP_i + TN_i)}{\sum_{i=1}^{C+1} (TP_i + TN_i + FP_i + FN_i)}, \quad (13)$$

where TP_i , TN_i , FP_i , and FN_i are true positive, true negative, false positive, and false negative of the i -th class. In hyperspectral image classification, we are interested in the accuracy of known land cover classes instead of the unknown. However, the open OA metric takes the accuracy of the unknown class into account. If the known classes only account for a small portion of the data, this metric will be dominated by the unknown classes.

The open OA is similar to the closed OA (the one normally used in classification) but includes the unknown class. For reference purposes, we show the closed OA below:

$$Closed\ OA = \frac{\sum_{i=1}^C (TP_i + TN_i)}{\sum_{i=1}^C (TP_i + TN_i + FP_i + FN_i)}. \quad (14)$$

3) *Micro F1 score*: A more reasonable indicator should be the micro F1 score, where we only consider the precision and recall of known classes. Note the F1 score of the unknown class should not be considered as pointed by [68]. With micro F1, the inclusion of unknown classes plays an important role in the precision scores. If unknown instances are classified into one of the known classes, precision will be decreased. The micro F1 score is calculated as follows,

$$F1 = \frac{2 \times Precision \times Recall}{Precision + Recall} \quad (15)$$

where,

$$Precision = \frac{\sum_{i=1}^C TP_i}{\sum_{i=1}^C (TP_i + FP_i)}, \quad (16)$$

$$Recall = \frac{\sum_{i=1}^C TP_i}{\sum_{i=1}^C (TP_i + FN_i)}. \quad (17)$$

4) *Mapping error*: The mapping error in a specific region is of direct interest to local governments, as policy-makers rely on food production data collected based on administrative regions to adapt their strategy. In this study, the mapping error is defined as,

$$Error = \frac{\sum_{i=1}^C |A_{p,i} - A_{gt,i}|}{\sum_{i=1}^C A_{gt,i}} \quad (18)$$

$$s.t. \quad A_i \geq 0, \quad \sum_{i=1}^{C+1} A_{p,i} = \sum_{i=1}^{C+1} A_{gt,i}$$

where $A_{p,i}$ is the predicted area of the i -th class, $A_{gt,i}$ is the ground truth area, C is the number of known classes, and $C+1$ class is the unknown. Note for the closed set classification, the mapping error should be,

$$Error_{close} = \frac{\sum_{i=1}^C |A_{p,i} - A_{gt,i}|}{\sum_{i=1}^C A_{gt,i}} \quad (19)$$

$$s.t. \quad A_i \geq 0, \quad \sum_{i=1}^C A_{p,i} = \sum_{i=1}^C A_{gt,i}.$$

If a model overestimates a land cover class, it will also underestimate another land cover class. Note in the open-world setting, the upper bound of the individual class in theory is $\sum_{i=1}^{C+1} A_{gt,i}$, whereas the upper bound for the closed world assumption is $\sum_{i=1}^C A_{gt,i}$. Therefore, the range of mapping error in the closed setting is 0–2, whereas the maximum error in open-world classification depends on the unknown instances included for evaluation and is calculated as $Error_{max} = 2 \times (1 + A_{gt,C+1} / \sum_{i=1}^C A_{gt,i})$.

Mapping error is not a point-by-point evaluation metric, meaning a zero error does not necessarily lead to zero classification confusion. However, for common multiclass scenarios, it is nearly impossible for a model to have a correct guess on the mapping area randomly. As a well-classified map is supposed to have a good estimation of the land cover area, mapping error is the most simple and direct metric to evaluate the accuracy of hyperspectral image classification, especially with the existence of unknown classes. Mapping error is also sensitive to imbalanced mapping (or in technical terms, the long tail), which is a great challenge when we are facing the open world [69]. We show a toy example in Table V, where three models achieve an identical OA but different errors. A good model, like Model 1, should carefully take care of the tail classes to reduce the mapping error. In contrast, an imbalanced model, although achieving the same OA, neglects the tail classes and thus leads to extreme overestimation and underestimation of the number and area of each land cover class.

TABLE V

A SIMPLE EXAMPLE ILLUSTRATING MAPPING ERROR’S SENSITIVITY TO IMBALANCED MAPPING (THE LONG TAIL). NOTE a/b INDICATES THE MODEL PREDICTS b INSTANCES BELONG TO THE CLASS, WHERE a INSTANCES ARE CORRECTLY CLASSIFIED.

	C1	C2	C3	OA	Error
GT	80	10	10	-	-
Model 1	70/80	5/10	5/10	80/100	0
Model 2	78/88	1/6	1/6	80/100	16/100
Model 3	80/100	0	0	80/100	40/100

C. Experimental setup

Experiments were carried out under both the few-shot context (20 training samples per class) and many-shot context (200 per class). The experiments were conducted using TensorFlow 1.9 [70] and Keras 2.1.6 [71] with Python 3.6 on a machine equipped with an Intel I5-8500 CPU, a Nvidia GTX 1080 Ti GPU and 32G RAM. The AdaDelta optimizer [72] is used for backpropagation in the training phase. The learning rate was set as 1.0 for the first 170 epochs and then, as 0.1 for another 30 epochs before the training stopped. We adopted the early stopping mechanism to accelerate the training. If the loss does not decrease for five epochs, the learning proceeds immediately to the next phase. To fully exploit the training samples, they were augmented horizontally, vertically, and diagonally; hence, the number of training samples NoS should be times four.

TABLE VI
NUMBER OF KNOWN AND NOVEL CLASSES (IN BRACKETS) AND PIXELS IN THE EXPERIMENTS.

		Pavia	Salinas	Indian
Almost perfect	Known Pixels (Classes)	42776 (9)	54129 (16)	8503 (8)
	Novel Pixels (Classes)	5163 (6)	5613 (2)	2007 (9)
OW1	Known Pixels (Classes)	14724 (3)	10716 (3)	2883 (3)
	Novel Pixels (Classes)	33215 (12)	49026 (15)	7627 (14)
OW2	Known Pixels (Classes)	26742 (3)	22483 (3)	4019 (3)
	Novel Pixels (Classes)	21197 (12)	37259 (15)	6491 (14)
OW3	Known Pixels (Classes)	11643 (3)	24069 (3)	3286 (3)
	Novel Pixels (Classes)	36296 (12)	35673 (15)	7224 (14)

In the experiments, the weights of classification and reconstruction losses are 0.5. The tail number is set as $NoS \times 4 \times 0.05 \times C$ for MDL4OW and $NoS \times 4 \times 0.05$ for MDL4OW/C, where NoS is the number of training samples per class, 4 is the number of augmentations of training samples, and C is the number of training classes. If the tail number is smaller than 20 for MDL4OW, then it is set as 20. The tail number here is not the global optimum and will be discussed in section IV-E. All results are reported from the average of ten random training sets. We compare our method with random forest, support vector machine, deep contextual CNN (DCCNN) [29], wide contextual residual network (WCRN) [73], the modified HResNet (the baseline of the proposed method) [43], and the state-of-the-art open-set method CROSR [52]. For open-set CNNs with confidence thresholding, the unknown probability is determined with a threshold of 0.5.

IV. RESULTS AND ANALYSIS

The experiments were conducted in two parts. In the first part, we evaluated the proposed method in an almost perfect classification system. Under this setting, only a small portion of the instances belong to unknown or novel due to the long-tail nature of the open world. In the second part, we selected some known classes as training data and the other classes as the unknown to evaluate the proposed method. This is the standard protocol for the open classification of daily images in computer vision, and the number of unknown classes greatly exceeds the known classes. However, the second setting is rare in real-world hyperspectral image classification. The number of known and novel classes and their supporting pixels in each setting are shown in Table VI.

A. With almost perfect classification systems

1) *Results on the University of Pavia dataset:* In the first experiment, we applied the proposed method to the popular benchmark data from the University of Pavia. In Tables VII and VIII, we show the overall OA, F1, mapping error, and class-wise F1 obtained with 20 and 200 training samples per class. Under the few-shot setting, MDL4OW achieved the best classification in terms of three evaluation metrics (85.07%, 0.9172, 14.03%), whereas CROSR achieved the second-best F1 score (84.66%, 0.9090, 14.95%). Under the many-shot setting, the best classification was obtained by MDL4OW/C. The OA and F1 are 90.53% and 0.9482, 1.87% and 0.0083 higher than the closed classification. When it

comes to the mapping error, the proposed method significantly outperformed conventional methods. The mapping error was reduced by 4.9% from 12.19% to 7.29%.

For illustrative purposes, we show the classification maps in Figure 4. We can see that the proposed method successfully identified the unknown classes (not annotated in the standard dataset) building-1, vehicles (the helicopter and some cars), the parking shed, and the swimming pool. Among the three open methods, only the CROSR identified building-2 as unknown, which is reflected in its high F1 score on the novel class. However, CROSR achieved a lower F1 in the second class meadows. This class covers a large area in the image, as indicated by the number of sample instances (Table II). As shown in the classification map (Figure 4 CROSR), on the lower side of the image, some meadows were misclassified as unknown by CROSR. CROSR is a centroid-based method and is sensitive to the intraclass variation. Meadows consist of over 18000 instances and have a large intraclass variation, limiting the performance of centroid-based methods. Large intraclass variation is common in remote sensing images. Therefore, the proposed MDL4OW is more robust and stable compared to CROSR.

2) *Results on the Salinas Valley dataset:* To evaluate the potential of the proposed method in estimating crop area, a popular agricultural dataset, the Salinas Valley, is used in the experiment. This dataset contains 16 agricultural classes, where some of the man-made materials are not considered (a road on the lower left and a water pool on the upper left). We manually annotated some of the man-made materials in white, as shown in Figure 5 reference map. The classification results are presented in Tables IX and X for few-shot and many-shot settings. Under the few-shot context, MDL4OW achieved the best classification result in terms of three evaluation metrics. Compared with the close classification, the OA increased by 4.94% from 82.46% to 87.40%; the F1 score increased by 0.0235 from 0.9038 to 0.9273. The mapping error is more sensitive to the unknown classes and reduced from 23.24% to 17.04%, up to 6%. This experiment strongly shows the potential of the proposed method in precisely estimating crop area. As for the many-shot setting, the class-wise MDL4OW/C achieved the best classification results, followed by MDL4OW. The mapping error was significantly reduced from 10.84% to 3.96%.

For illustrative purposes, we show the classification maps obtained from the many-shot setting in Figure 5. We can see that a lot of known instances (the lower part) are misclassified as unknown with the CROSR method. In contrast, the proposed MDL4OW successfully identified the unknown (a road on the lower left and a water pool on the upper left) while maintaining high accuracy on the known classes. As in remotely sensed hyperspectral images, the unknown should only count for a small portion of the image; the proposed method is more suitable for the classification of hyperspectral data.

3) *Results on the Indian Pines dataset:* To show the generalization of the proposed method, another popular dataset, Indian Pines, is tested. This dataset, as shown in the false color map in Figure 6, mainly covers an agricultural region. In

the standard 16-class reference map, one non-agricultural class exists. However, the road on the upper side of the image is not represented in the reference data. It should not be considered as an agricultural class. As mentioned before, since some of the land covers in this dataset consist of very few samples, we only included eight classes as the training set following [29]. The remaining 8+1 classes were naturally considered as unknown. The results are reported in Tables XI and XII.

Under the few-shot context, the three open methods are competitive and resulted in a mapping error of 28%–29%, 3–4% lower compared to the closed error of 33.27%, whereas the proposed MDL4OW is slightly better. As for the many-shot setting, the class-wise MDL4OW/C obtained the best classification result in three evaluation metrics. The OA and F1 are 82.61% and 0.9001, 2.47% and 0.0104 higher than the closed classification. The mapping error is more sensitive, and is 16.00%, 7.60% lower than the baseline.

We show the classification maps obtained using 200 samples per class in Figure 6. The road on the upper side of the image is successfully identified as unknown by the proposed method, both MDL4OW and MDL4OW/C. The close CNN classified it as one of the agricultural classes, soybean-mintill, leading to its overestimation. CROSR failed to recognize the road as unknown. From the classification maps, we can see that most man-made materials unrelated to crops can be identified as unknown by the proposed method, showing its promise in precise crop mapping.

4) *Threshold analysis:* We show a threshold analysis under the few-shot context in Figure 7 to demonstrate that a) SoftMax confidence thresholding is not enough for detecting the unknown, and b) MDL4OW is robust to the threshold setting (z). From Figure 7 we can see that with a larger threshold, the F1 score first slightly improves and then drops sharply. A low SoftMax probability indicates the classifier is uncertain with its decision, but uncertainty is not equal to unknown. A sample instance that is difficult to classify may be the valuable instance close to the decision boundary between two classes (the valuable sample in active learning) [46].

B. Comparison with other methods

In Table XIII, we compare the proposed methods with other competitors in terms of closed OA and open OA using 200 samples per class. The comparison is based on the Pavia and Salinas data. We do not compare the results on the Indian data since the used known classes are different with other studies. Closed OA is calculated based on known classes without considering the existence of unknown class. Open OA includes the unknown class. It is easy to convert a closed OA to open OA once the unknown instances are determined from a reference map. Besides two non-deep methods (RF and SVM), we also include eight deep learning methods and three deep learning-based few-shot methods. They are DCCNN [29], WCRN [73], HResNet (baseline of the proposed method), CNN [74], R-PCA-CNN [42], CNN-PPF [75], C-CNN [76], SSRN [35], DFSL+NN [36], DFSL+SVM [36], and SS-RN [37].

MDL4OW/C achieves the best open OA, followed by MDL4OW. Those closed methods lack the ability to tell the

TABLE VII

CLASSIFICATION ACCURACY USING 20 SAMPLES PER CLASS ON THE UNIVERSITY OF PAVIA DATASET. * TOP-1 SOFTMAX PROBABILITY < 0.5 IS CONSIDERED AS UNKNOWN. ERROR (%): THE SMALLER THE BETTER; ELSE: THE LARGER THE BETTER.

	Close					Open					
	RF	SVM	DCCNN [29]	WCRN [73]	HResNet [43]	DCCNN*	WCRN*	HResNet*	CROSR [52]	MDL4OW	MDL4OW/C
1	76.34	75.82	84.60	85.50	91.66	84.60	85.52	91.72	85.87	91.56	89.78
2	69.17	81.67	91.15	93.77	95.57	91.17	93.76	95.57	93.37	95.57	93.84
3	51.82	60.32	57.50	67.46	79.82	57.78	67.71	80.15	83.41	82.70	81.95
4	68.44	78.96	89.98	91.09	92.16	90.08	91.23	92.35	92.96	91.69	89.47
5	64.38	67.13	84.71	89.02	88.46	84.92	89.11	88.78	95.83	90.27	91.88
6	40.06	53.04	65.76	67.50	74.81	65.81	67.68	75.00	77.91	76.37	78.32
7	61.01	62.79	64.78	72.19	72.24	65.03	72.59	72.94	90.57	75.71	76.01
8	67.41	75.17	72.24	70.35	82.53	72.41	70.50	82.62	84.38	83.93	80.42
9	99.79	99.88	91.27	91.23	86.63	91.51	91.46	87.25	93.19	86.72	84.51
Novel	0.00	0.00	0.00	0.00	0.00	2.50	2.73	4.87	57.21	32.77	42.06
OA (%)	60.36±2.19	69.28±3.22	76.81±2.78	79.40±1.56	83.52±1.42	76.90±2.82	79.44±1.56	83.73±1.36	84.66±3.61	85.07±1.58	83.35±2.43
F1×100	75.25±1.71	81.81±2.30	86.86±1.81	88.51±0.97	91.01±0.84	86.89±1.83	88.51±0.97	91.11±0.81	90.90±2.28	91.72±0.96	90.44±1.50
Error (%)	44.22±9.17	30.27±6.26	24.05±6.67	17.19±4.40	16.59±3.31	23.81±6.72	16.93±4.51	16.31±3.22	14.95±5.23	14.03±3.69	14.31±3.69

TABLE VIII

CLASSIFICATION ACCURACY USING 200 SAMPLES PER CLASS ON THE UNIVERSITY OF PAVIA DATASET. * TOP-1 SOFTMAX PROBABILITY < 0.5 IS CONSIDERED AS UNKNOWN. ERROR (%): THE SMALLER THE BETTER; ELSE: THE LARGER THE BETTER.

	Close					Open					
	RF	SVM	DCCNN [29]	WCRN [73]	HResNet [43]	DCCNN*	WCRN*	HResNet*	CROSR [52]	MDL4OW	MDL4OW/C
1	82.77	83.22	94.90	93.44	95.29	94.88	93.46	95.34	93.05	93.68	94.54
2	83.73	92.93	97.84	98.56	99.03	97.85	98.56	99.04	96.64	99.03	98.81
3	72.67	76.75	78.36	93.00	93.75	78.54	93.03	93.82	93.96	97.39	96.72
4	83.37	92.24	95.83	97.01	90.16	95.89	97.04	90.24	95.02	90.42	90.61
5	75.79	75.08	90.53	94.61	88.74	90.61	94.64	88.86	96.08	98.11	97.47
6	52.88	73.54	76.59	77.48	83.93	76.66	77.50	84.01	86.55	85.23	86.29
7	72.67	79.91	84.09	75.77	75.59	84.35	75.83	75.77	96.17	81.93	80.56
8	80.28	83.63	88.75	87.48	96.65	88.94	87.53	96.71	95.04	94.81	95.74
9	99.51	99.92	97.31	96.04	94.46	97.39	96.07	94.61	96.29	95.21	94.52
Novel	0.00	0.00	0.00	0.00	0.00	1.85	0.52	1.91	61.70	38.43	45.94
OA (%)	72.77±0.88	81.36±0.43	86.55±0.50	87.39±0.18	88.66±0.12	86.58±0.54	87.41±0.17	88.76±0.13	90.39±0.67	90.17±0.13	90.53±0.62
F1×100	84.24±0.59	89.72±0.26	92.78±0.29	93.27±0.10	93.99±0.07	92.80±0.31	93.28±0.10	94.03±0.07	94.51±0.37	94.66±0.08	94.82±0.33
Error (%)	29.87±2.34	14.72±1.62	13.76±1.14	12.66±0.48	12.19±0.18	13.56±1.15	12.61±0.49	12.06±0.18	7.39±1.44	8.36±0.04	7.29±0.95

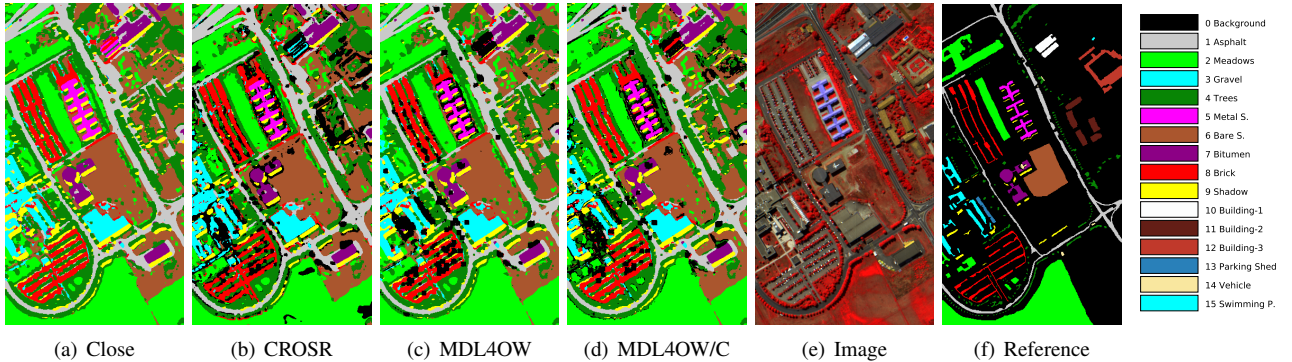


Fig. 4. Classification maps of the University of Pavia. Known classes: 1-9; unknown classes: 10-15. In the classification maps, those masked with black color are identified as unknown by the proposed method.

unknown from known classes and therefore achieve a low open OA. Take the SSRN [35] as an example. It achieves the highest closed OA on the Salinas data (98.68%), but only obtains an open OA of 89.41%. MDL4OW/C obtains the highest open OA (94.34%), whereas MDL4OW obtains the second highest open OA (93.73%) and a reasonable closed OA (96.37%). It should note that although open methods are promising in identifying the novel class, they inevitably lead to either a large or a slightly decrease in the closed OA, since the closed methods do not bother with the novel class. The trade-off here is similar to target detection [77]. As the novel class is inevitable in the real world, a method that is capable of identifying the unknown and maintaining good performance on the known classes is essential. The proposed MDL4OW achieves a good trade-off here if we look at both the closed

OA and open OA.

C. With imperfect classification systems

In this section, we evaluate the proposed method with imperfect classification systems. Land cover classification systems are multilevel. For fine-grained crop mapping, each crop can be categorized as an individual class, but they all belong to a larger class, vegetation. The hierarchy of land cover classification systems makes it easy to distinguish between impervious and vegetation but difficult to distinguish between meadows and trees. Therefore, we designed a series of experiments, where we selected some classes into training, as shown in Table XIV. Some of them are all from impervious classes, leading to a classification system without vegetation (Pavia

TABLE IX
CLASSIFICATION ACCURACY USING 20 SAMPLES PER CLASS ON THE SALINAS VALLEYS DATASET. * TOP-1 SOFTMAX PROBABILITY < 0.5 IS CONSIDERED AS UNKNOWN. ERROR (%): THE SMALLER THE BETTER; ELSE: THE LARGER THE BETTER.

	Close					Open					
	RF	SVM	DCCNN [29]	WCRN [73]	HResNet [43]	DCCNN*	WCRN*	HResNet*	CROSR [52]	MDL4OW	MDL4OW/C
1	97.25	97.64	80.93	92.02	99.86	81.02	92.09	99.86	93.24	94.58	94.49
2	97.80	97.90	85.30	98.05	99.74	85.21	98.07	99.77	92.60	96.95	97.99
3	80.22	91.99	73.05	89.78	97.90	72.42	89.74	97.93	93.27	98.58	95.42
4	70.62	75.44	71.92	74.86	69.31	72.03	74.99	69.42	96.23	97.22	95.93
5	90.24	92.25	77.16	71.11	67.05	77.36	71.26	67.13	93.86	83.50	85.75
6	81.66	90.72	95.75	93.97	97.49	95.83	94.07	97.60	93.17	95.19	99.12
7	96.87	98.49	98.09	98.38	98.59	98.09	98.37	98.55	94.67	96.31	95.59
8	62.70	70.79	39.08	71.62	74.71	35.33	71.44	74.72	74.66	75.22	75.18
9	93.38	87.11	89.36	94.57	97.24	89.48	94.57	97.26	95.12	98.02	96.81
10	74.87	77.92	81.30	84.25	90.97	81.57	84.32	91.04	89.11	91.89	90.28
11	62.30	61.27	63.14	78.83	73.03	63.61	79.50	73.35	84.83	82.37	81.84
12	92.82	94.40	91.20	98.51	99.54	91.93	98.52	99.55	93.61	99.89	98.70
13	89.68	93.88	90.60	97.28	99.16	91.83	97.29	99.22	94.80	99.93	99.56
14	80.83	88.93	92.94	94.30	98.54	93.20	94.42	98.58	95.37	98.83	96.65
15	56.67	62.46	54.08	65.87	77.40	49.56	65.96	77.40	76.45	77.49	77.31
16	84.67	87.57	93.90	80.50	90.89	94.11	80.67	90.94	94.64	99.14	95.43
Novel	0.00	0.00	0.00	0.00	0.00	4.21	2.32	1.69	64.94	74.39	75.97
OA (%)	74.50±1.63	78.02±1.76	70.48±3.19	78.74±1.69	82.46±1.65	68.84±5.69	78.69±1.77	82.51±1.64	84.27±1.29	87.40±1.60	87.12±1.57
F1×100	85.38±1.08	87.64±1.11	82.64±2.17	88.09±1.06	90.38±1.39	81.35±4.19	88.05±1.11	90.41±1.41	90.57±0.85	92.73±1.36	92.43±1.37
Error (%)	19.91±5.19	17.37±4.50	36.71±14.27	21.12±6.09	23.24±5.59	36.62±13.66	20.97±6.14	23.15±5.59	18.68±2.12	17.04±5.37	18.20±5.67

TABLE X
CLASSIFICATION ACCURACY USING 200 SAMPLES PER CLASS ON THE SALINAS VALLEYS DATASET. * TOP-1 SOFTMAX PROBABILITY < 0.5 IS CONSIDERED AS UNKNOWN. ERROR (%): THE SMALLER THE BETTER; ELSE: THE LARGER THE BETTER.

	Close					Open					
	RF	SVM	DCCNN [29]	WCRN [73]	HResNet [43]	DCCNN*	WCRN*	HResNet*	CROSR [52]	MDL4OW	MDL4OW/C
1	99.66	99.83	84.00	87.70	91.18	84.10	87.81	91.30	96.58	94.01	94.60
2	99.63	99.73	99.35	99.99	99.93	99.40	99.99	99.94	97.05	97.74	99.04
3	91.53	97.53	93.92	88.70	88.94	94.18	88.79	89.02	96.25	92.18	98.45
4	71.94	81.47	88.35	80.35	64.48	88.37	80.45	64.53	97.12	98.19	98.55
5	92.54	85.04	73.29	74.36	87.25	73.37	74.46	87.36	96.97	95.17	96.47
6	85.91	93.21	98.14	97.94	98.80	98.19	98.00	98.83	96.82	99.73	97.26
7	98.56	99.34	99.51	99.68	95.57	99.53	99.68	95.60	96.86	97.16	97.87
8	75.99	82.22	80.59	85.64	90.95	80.54	85.65	90.95	90.17	91.71	92.55
9	96.76	94.76	94.99	96.03	95.99	95.01	96.05	96.01	96.36	97.44	97.72
10	74.97	74.49	89.85	89.02	93.51	90.09	89.18	93.61	94.35	96.24	97.39
11	73.20	91.95	84.13	99.05	96.55	84.42	99.08	96.61	96.35	97.48	97.53
12	97.25	98.92	99.69	99.91	99.79	99.71	99.91	99.80	96.76	99.85	97.76
13	97.16	98.85	99.68	99.75	99.56	99.71	99.76	99.61	97.15	99.91	99.12
14	91.60	94.26	94.74	99.19	97.70	95.03	99.21	97.81	96.12	98.79	98.51
15	67.87	75.37	79.08	82.16	91.07	79.13	82.21	91.08	88.70	91.18	89.99
16	93.92	94.59	98.40	93.94	92.84	98.47	93.97	92.86	96.83	99.61	98.62
Novel	0.00	0.00	0.00	0.00	0.00	2.84	1.95	1.57	75.26	76.87	83.32
OA (%)	80.85±0.50	83.87±0.30	84.08±2.19	85.72±1.60	88.14±1.90	84.16±2.16	85.81±1.60	88.22±1.90	91.82±0.52	93.73±0.80	94.34±0.61
F1×100	89.41±0.30	91.23±0.17	91.34±1.32	92.30±0.95	93.70±1.50	91.37±1.31	92.35±0.95	93.73±1.51	95.29±0.31	96.53±0.60	96.82±0.71
Error (%)	15.16±2.08	11.53±0.90	17.31±7.29	14.30±5.24	10.84±4.50	17.12±7.30	14.21±5.24	10.76±4.50	6.98±0.83	4.63±2.79	3.96±2.61

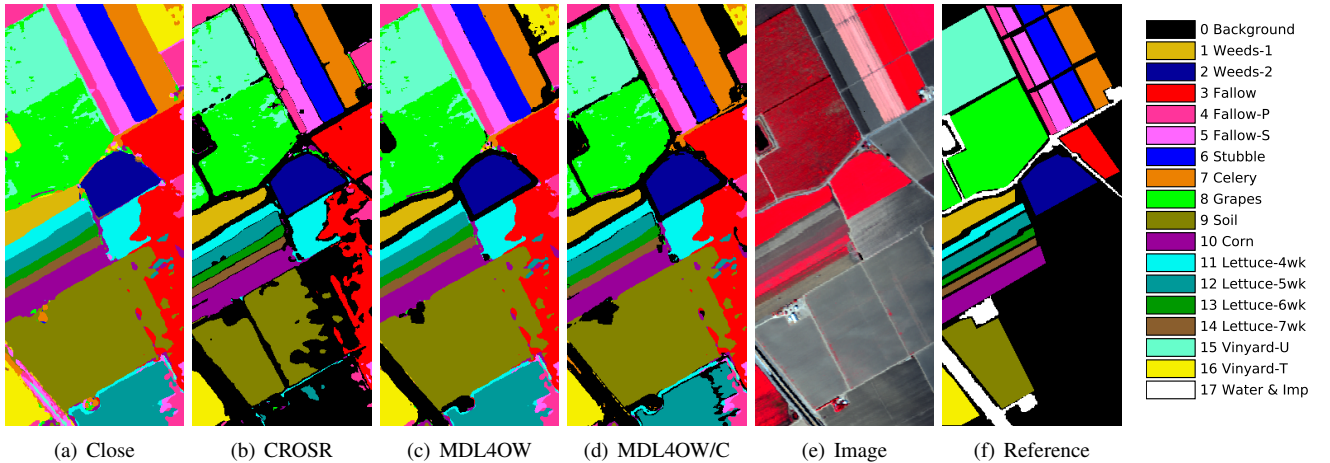


Fig. 5. Classification maps of the Salinas Valley. Known classes: 1-16; unknown classes: 17. In the classification maps, those masked with black color are identified as unknown by the proposed method.

OW3); some of them are the same crop type with a minor difference in terms of growing weeks (Salinas OW1).

A classification system lacking the basic elements (imperious, vegetation, and water) is extremely incomplete and in

need of the proposed method to reject the unknown classes. For a complete classification system, this task will be extremely difficult, as the interclass variation might be too small. For the experimental details, we select 3, 6, and 3 training

TABLE XI

CLASSIFICATION ACCURACY USING 20 SAMPLES PER CLASS ON THE INDIAN PINES DATASET. * TOP-1 SOFTMAX PROBABILITY < 0.5 IS CONSIDERED AS UNKNOWN. ERROR (%): THE SMALLER THE BETTER; ELSE: THE LARGER THE BETTER.

	Close					Open					
	RF	SVM	DCCNN [29]	WCRN [73]	HResNet [43]	DCCNN*	WCRN*	HResNet*	CROSR [52]	MDL4OW	MDL4OW/C
1	47.95	48.43	50.24	62.79	73.48	50.23	62.92	73.54	71.58	74.89	74.51
2	46.15	41.52	39.08	51.76	69.12	39.42	52.22	69.35	68.63	68.22	68.45
3	35.75	44.91	62.45	62.52	67.03	62.70	63.48	67.55	70.05	65.12	66.34
4	82.43	89.64	90.58	90.24	89.57	90.90	90.88	89.79	88.04	89.61	89.24
5	53.92	54.54	46.07	60.47	76.42	45.93	61.08	76.58	75.03	76.79	78.21
6	54.45	54.87	56.35	64.98	77.06	56.28	65.06	77.01	74.43	77.23	76.55
7	37.06	45.99	43.56	48.42	65.57	43.79	48.92	66.10	66.99	65.50	66.01
8	87.23	83.34	75.06	84.99	84.49	75.40	85.52	84.64	87.85	84.34	83.85
Novel	0.00	0.00	0.00	0.00	0.00	6.98	9.70	3.11	36.16	21.18	27.93
OA (%)	49.27±1.48	51.01±1.90	50.99±2.98	58.67±2.10	67.98±2.58	51.35±2.87	59.35±2.35	68.14±2.57	68.49±3.94	68.92±3.26	69.00±3.90
F1×100	66.00±1.33	67.53±1.68	67.49±2.61	73.93±1.68	80.91±1.87	67.43±2.67	74.12±1.81	80.95±1.87	79.83±2.40	80.99±2.19	80.73±2.42
Error (%)	46.48±8.97	41.74±9.19	48.43±9.27	38.26±8.64	33.27±10.10	47.11±11.16	36.71±9.62	32.62±9.93	28.90±11.85	28.32±10.74	28.37±11.30

TABLE XII

CLASSIFICATION ACCURACY USING 200 SAMPLES PER CLASS ON THE INDIAN PINES DATASET. * TOP-1 SOFTMAX PROBABILITY < 0.5 IS CONSIDERED AS UNKNOWN. ERROR (%): THE SMALLER THE BETTER; ELSE: THE LARGER THE BETTER.

	Close					Open					
	RF	SVM	DCCNN [29]	WCRN [73]	HResNet [43]	DCCNN*	WCRN*	HResNet*	CROSR [52]	MDL4OW	MDL4OW/C
1	76.23	78.72	77.63	94.14	94.97	77.72	94.22	95.06	94.34	95.31	95.03
2	72.88	72.83	73.07	84.24	82.66	72.52	84.40	82.77	82.89	83.26	83.47
3	54.32	54.74	64.01	71.76	85.79	64.51	72.31	86.31	86.05	85.33	85.66
4	91.77	93.89	95.12	95.01	95.17	95.15	95.05	95.23	95.91	94.88	95.31
5	78.01	77.04	81.76	91.28	93.79	82.16	91.65	94.08	93.97	94.08	94.52
6	77.84	78.80	82.44	94.80	87.64	81.57	94.90	87.80	87.12	88.82	88.67
7	55.72	85.09	81.23	85.49	82.91	81.86	85.95	83.44	88.76	84.98	88.35
8	79.32	86.43	75.90	75.73	86.91	76.03	76.04	87.16	88.91	87.58	87.70
Novel	0.00	0.00	0.00	0.00	0.00	3.86	4.76	4.50	22.09	32.21	33.58
OA (%)	66.73±0.58	70.53±0.53	70.97±6.56	79.13±0.54	80.14±0.40	70.41±7.29	79.58±0.56	80.57±0.46	81.55±1.53	82.23±1.64	82.61±1.91
F1×100	80.04±0.04	82.72±0.36	82.84±4.62	88.35±0.34	88.97±0.24	82.32±5.24	88.57±0.35	89.19±0.27	89.54±0.79	89.79±0.89	90.01±1.02
Error (%)	34.95±1.70	28.13±4.02	33.75±8.95	24.54±1.81	23.60±0.23	33.22±9.02	23.95±1.81	23.00±0.31	18.76±2.17	16.26±1.49	16.00±2.36

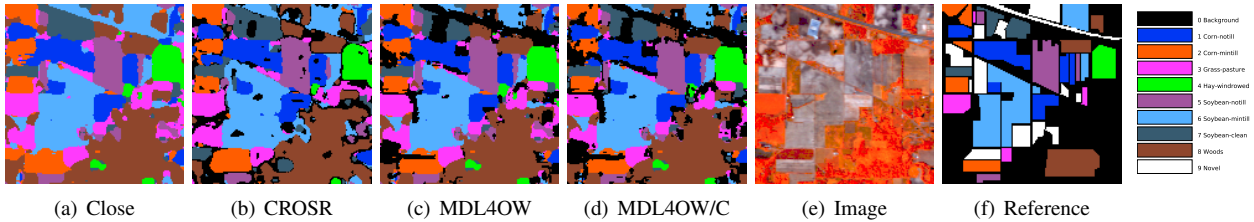


Fig. 6. Classification maps of the Indian Pines. Known classes: 1-8; unknown classes: 9. In the classification maps, those masked with black color are identified as unknown by the proposed method.

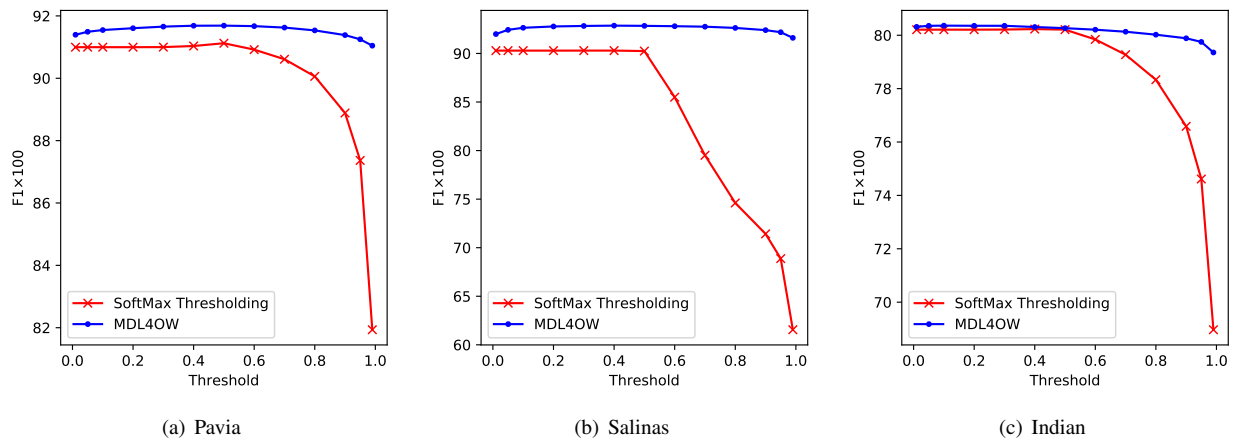


Fig. 7. Confidence threshold analysis in terms of F1 score under the few-shot setting.

classes for the Pavia, Salinas, and Indian datasets, respectively, and all classes as the test set, as shown in Table XIV, leading to openness values of 42.3%, 29.3%, and 45.2%, respectively.

Three open-world (OW) scenarios are tested for each dataset: some are complete, and some are incomplete (denoted with *).

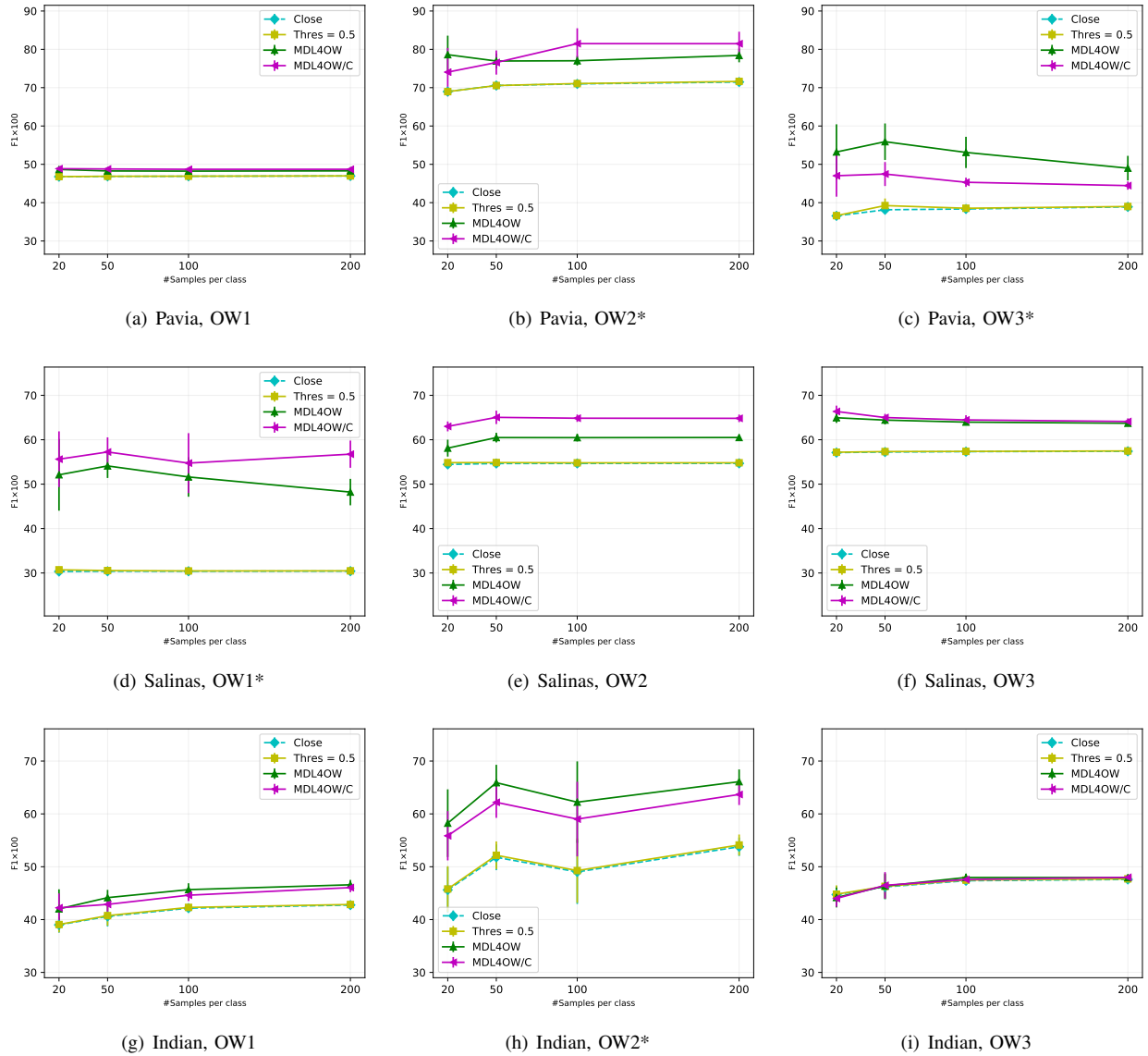


Fig. 8. F1 as a function of the number of training samples per class. * incomplete classification system.

TABLE XIII

COMPARISON WITH OTHER METHODS IN TERMS OF CLOSED OA (%) AND OPEN OA (%). * TOP-1 SOFTMAX PROBABILITY < 0.5 IS CONSIDERED AS UNKNOWN.

Method		Pavia University		Salinas Valley	
		Closed OA	Open OA	Closed OA	Open OA
Non-deep	RF	81.56±0.99	72.77±0.88	89.24±0.55	80.85±0.50
	SVM	91.18±0.48	81.36±0.43	92.60±0.34	83.87±0.30
Close	DCCNN [29]	96.99±0.56	86.55±0.50	92.84±2.41	84.08±2.19
	WCRN [73]	97.94±0.20	87.39±0.18	94.66±1.76	85.72±1.60
	HResNet	99.36±0.15	88.66±0.12	97.39±0.64	88.14±1.90
	CNN [74]	87.90	78.43	90.25	81.77
	R-PCA-CNN [42]	94.38	84.62	92.39	83.71
	CNN-PPF [75]	96.48	86.09	94.80	85.89
	C-CNN [76]	98.41	87.81	97.42	88.27
SSRN [35]	99.79	89.04	98.68	89.41	
Few-shot	DFSL+NN [36]	97.85	87.31	97.78	88.59
	DFSL+SVM [36]	98.62	88.00	97.81	88.62
	SS-RN [37]	99.69	88.95	98.62	89.35
Open	DCCNN*	96.92±0.59	86.58±0.54	92.77±2.41	84.16±2.16
	WCRN*	97.93±0.20	87.41±0.17	94.65±1.76	85.81±1.60
	HResNet*	99.35±0.14	88.76±0.13	97.38±0.64	88.22±1.90
	CROSR [52]	96.67±0.25	90.39±0.67	94.75±0.53	91.82±0.52
	MDL4OW	97.93±0.26	90.17±0.13	96.37±0.80	93.73±0.80
	MDL4OW/C	97.23±0.37	90.53±0.62	94.99±0.63	94.34±0.61

The F1 score as a function of the number of training samples per class is shown in Figure 8. As shown, the performance of the proposed method varies. For the incomplete classification systems (with *), the proposed MDL4OW significantly improves the classification in terms of the F1 score. For the others, the improvement is less significant. Interestingly, the accuracy in terms of F1 is not affected by the number of training samples per class. In this case, collecting more samples cannot enhance the classification in the OW with the existence of unknown classes. This provides the insight that, for hyperspectral image classification, a machine learning model needs to identify the unknown classes; otherwise the classification accuracy cannot be improved by simply adding more data, as those unknowns will decrease the precision because the model is forced to assign a label.

More details compared with the state-of-the-art methods in terms of the three evaluation metrics (OA, F1, and mapping error) are shown in Tables XV, XVI, and XVII for the

TABLE XIV
SELECTED IMPERFECT CLASSIFICATION SYSTEMS. THE NUMBER IS THE CLASS INDEX. * INCOMPLETE CLASSIFICATION SYSTEM.

Dataset	#Train	#Test	Openness (%)	OW1	OW2	OW3
Pavia	3	15	42.3	[1, 4, 6] Asphalt, Trees, Bare S. [1, 2, 11, 12, 13, 14]*	[2, 4, 6]* Meadows, Trees, Bare S. [1, 3, 6, 9, 11, 15]	[1, 7, 8]* Asphalt, Bitumen, Brick [2, 5, 9, 10, 13, 15]
Salinas	6	18	29.3	Weed-1, Weed-2, Lett.-4wk Lett.-5wk, Lett.-6wk, Lett.-7wk [1, 3, 5]	Weed-1, Fallow, Stubble Soil, Lett.-4wk, Viny.-U [5, 6, 7]*	Weed-2, Fallow-S, Soil Corn, Lett.-6wk, Viny.-U [1, 7, 8]
Indian	3	17	45.2	Corn-n., Grass, Soybean-n.	Soybean-n., Soybean-m., Soybean-c.	Corn-n., Soybean-c., Woods

TABLE XV

CLASSIFICATION COMPARISON ON THE PAVIA DATASET: OA (%), $F1 \times 100$ AND MAPPING ERROR (%). OPENNESS = 42.3%. * INCOMPLETE CLASSIFICATION SYSTEM. DUE TO THE EXISTENCE OF UNKNOWN INSTANCES, THE MAXIMUM ERROR CAN BE LARGER THAN 100% AND IS CALCULATED AS $Error_{max} = 2 \times (1 + A_{gt,C+1} / \sum_{i=1}^C A_{gt,i})$.

	Method	Few-shot			Many-shot		
		OA	F1	Error	OA	F1	Error
OW1	Close	30.53	46.78	225.58	30.68	46.96	225.58
	Softmax	30.59	46.80	225.38	30.75	46.98	225.35
	CROSR	38.94	25.53	196.67	38.17	25.32	201.25
	MDL4OW	39.94	48.66	187.63	38.18	48.29	189.38
	MDL4OW/C	38.85	48.86	189.62	36.96	48.71	200.18
OW2*	Close	52.65	68.98	82.33	55.61	71.47	79.29
	Softmax	52.65	68.96	82.19	55.94	71.62	78.69
	CROSR	33.67	29.56	114.32	28.12	22.85	116.41
	MDL4OW	71.71	78.60	44.03	70.21	78.41	48.26
	MDL4OW/C	63.99	74.06	58.60	75.00	81.48	41.98
OW3*	Close	22.37	36.56	311.74	24.15	38.90	311.74
	Softmax	22.62	36.61	310.40	24.46	38.99	310.43
	CROSR	25.19	19.26	307.32	30.23	18.78	287.55
	MDL4OW	61.44	53.22	141.99	52.54	49.00	182.28
	MDL4OW/C	50.19	47.02	193.03	41.04	44.45	237.39

TABLE XVI

CLASSIFICATION COMPARISON ON THE SALINAS DATASET: OA (%), $F1 \times 100$ AND MAPPING ERROR (%). OPENNESS = 29.3%. * INCOMPLETE CLASSIFICATION SYSTEM. DUE TO THE EXISTENCE OF UNKNOWN INSTANCES, THE MAXIMUM ERROR CAN BE LARGER THAN 100% AND IS CALCULATED AS $Error_{max} = 2 \times (1 + A_{gt,C+1} / \sum_{i=1}^C A_{gt,i})$.

	Method	Few-shot			Many-shot		
		OA	F1	Error	OA	F1	Error
OW1*	Close	17.87	30.33	457.54	17.93	30.41	457.50
	Softmax	19.34	30.71	449.38	18.21	30.48	455.98
	CROSR	73.24	17.91	144.16	51.82	7.17	257.43
	MDL4OW	66.96	52.11	178.38	63.09	48.22	199.96
	MDL4OW/C	71.80	55.63	151.29	73.16	56.75	145.44
OW2	Close	37.40	54.44	165.72	37.63	54.68	165.72
	Softmax	38.42	54.84	162.94	37.96	54.81	164.85
	CROSR	45.09	31.09	144.81	42.29	29.66	153.30
	MDL4OW	47.41	58.11	135.71	52.16	60.50	124.12
	MDL4OW/C	57.75	63.00	106.92	60.05	64.82	102.06
OW3	Close	39.97	57.12	148.21	40.26	57.41	148.21
	Softmax	40.16	57.19	147.71	40.43	57.47	147.79
	CROSR	48.92	32.17	126.45	50.71	33.03	122.28
	MDL4OW	58.12	64.95	96.97	55.39	63.72	105.17
	MDL4OW/C	61.71	66.37	83.93	55.96	64.11	105.01

TABLE XVII

CLASSIFICATION COMPARISON ON THE INDIAN DATASET: OA (%), $F1 \times 100$ AND MAPPING ERROR (%). OPENNESS = 45.2%. * INCOMPLETE CLASSIFICATION SYSTEM. DUE TO THE EXISTENCE OF UNKNOWN INSTANCES, THE MAXIMUM ERROR CAN BE LARGER THAN 100% AND IS CALCULATED AS $Error_{max} = 2 \times (1 + A_{gt,C+1} / \sum_{i=1}^C A_{gt,i})$.

	Method	Few-shot			Many-shot		
		OA	F1	Error	OA	F1	Error
OW1	Close	24.24	39.00	264.55	27.19	42.76	264.55
	Softmax	24.50	39.07	263.34	27.49	42.85	263.46
	CROSR	36.25	41.54	206.9	31.96	44.31	245.84
	MDL4OW	36.99	42.02	205.39	41.78	46.58	198.04
	MDL4OW/C	36.92	42.22	207.55	37.77	46.05	221.29
OW2*	Close	29.65	45.61	171.87	36.80	53.78	161.84
	Softmax	30.33	45.80	169.56	37.65	54.12	159.58
	CROSR	34.77	18.27	144.18	42.55	18.61	109.71
	MDL4OW	60.08	58.24	87.09	64.31	66.10	79.19
	MDL4OW/C	54.84	55.86	104.96	58.89	63.68	100.12
OW3	Close	28.82	44.73	219.84	31.23	47.60	219.84
	Softmax	29.04	44.80	219.09	31.54	47.71	218.86
	CROSR	42.13	48.29	160.43	49.63	45.11	123.94
	MDL4OW	33.08	46.18	190.60	35.97	47.95	193.51
	MDL4OW/C	31.06	46.00	201.28	34.02	48.00	205.96

Pavia, Salinas, and Indian datasets, respectively. The best classification is highlighted in bold in each setting. In most cases, the proposed method outperforms the competitors.

Although, in theory, MDL4OW is supposed to have a better classification compared to MDL4OW/C under the few-shot context, in this experiment, MDL4OW/C can sometimes achieve very good results. The problem of the class-wise method is that, when it comes to few-shot learning, there are not enough instances to estimate the distribution. But if the openness is large, meaning the unknown data exceeds the known data (this is rare in hyperspectral image classification, since it is not difficult to define an acceptable classification system where there are more knowns than unknowns), then the overlapped region of the known and unknown instances would be large enough. In this case, the tail size of the known instances is large enough; even a small set of training data can achieve a reasonable estimation of the distribution. More details about the tail analysis can be found in section IV-E

D. Reconstruction analysis

Since a critical assumption of the proposed method is that the unknown classes will be poorly reconstructed, we show the original and reconstructed spectral profiles of the Pavia dataset in Figure 9. Trees are one of the known classes in the Pavia dataset. The reconstructed spectral profiles remain as the classic vegetation curve. The reconstructed profiles are tighter, indicating less intraclass variation. Building-1 is one of the unknown classes. We can see that the reconstructed spectral profiles are very different from the original ones. This analysis confirms the assumption that the unknown classes

are poorly reconstructed, indicating the effectiveness of the proposed method.

E. Sensitivity of the tail number

The tail number τ is an important factor in the proposed method and should be set carefully. We show the OA, F1, and mapping error as a function of the tail number under the few-shot context in Figure 10. We can see that the proposed MDL4OW is less sensitive to the tail number than MDL4OW/C. The former is conducted on all training data and free from estimating the class centroid in a class-wise fashion. Under the few-shot context, since the number of training samples per class is limited (20 per class), it is difficult to apply the EVT to estimate the extreme cases. Note, we augmented the training samples so the number of training

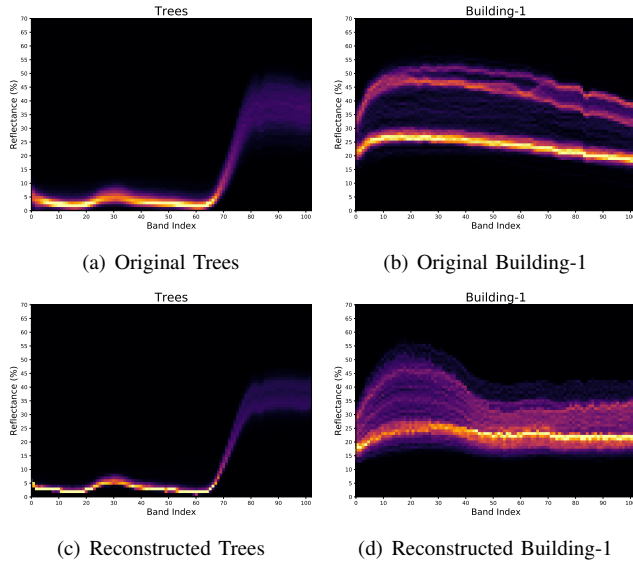


Fig. 9. Density of the original (top) and reconstructed (bottom) spectral profiles of the University of Pavia data set. A brighter color indicates that more sample instances have the similar spectral profiles.

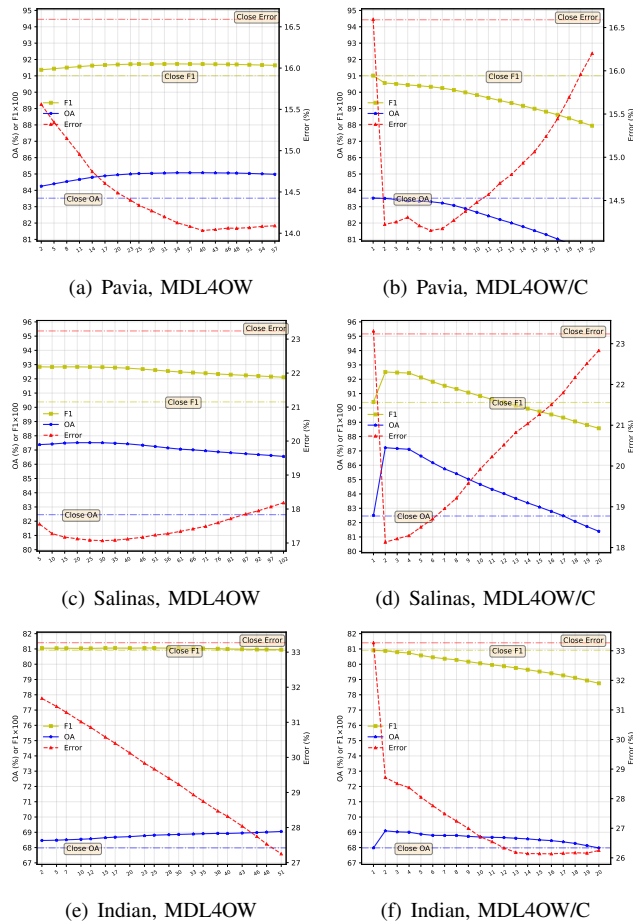


Fig. 10. Sensitivity of the tail number τ . Note we augmented the training samples in the experiments, so the size of training set should times 4.

samples per class should $\times 4$, which in a way eases the problem.

For the Pavia and Indian datasets, the F1 scores are already

lower than the closed classification when the tail size τ is 2 (EVT does not work when the tail size τ is 1, because one instance cannot estimate a distribution). For the Salinas dataset, the safe range of the tail number in terms of F1 is 2–12, where $\tau = 2$ is the optimum, showing that a smaller tail should be set, but there are not enough instances in the class-wise method.

Comparing three evaluation metrics, F1 is always higher than OA and is stricter in evaluation. Take Salinas MDL4OW/C as an example. F1 is lower than the baseline when the tail number is greater than 12, but OA is still higher than the baseline until the tail number is greater than 17. Recall that the F1 score is calculated based on the known classes, and OA includes the unknown class. When the tail size is between 12 and 17, the accuracy of the unknown class makes OA above the baseline. But, since we care more about the known classes than the unknown, it makes more sense to use the F1 score instead of OA. As for mapping error, its real meaning is the average error on the predicted number of all known classes (i.e., land cover area) and is of direct interest to local governments. We can see that it benefits the most from the proposed method where the unknown classes are considered. The evaluation of open-set classification is still an ongoing problem [68]. Although OA and F1 are the most common evaluation metrics, as the real-world meaning of mapping error is straightforward in hyperspectral image classification, it can be used as another standard metric for this application.

To conclude, the proposed method MDL4OW achieved state-of-the-art results in terms of all three of the evaluation metrics under the few-shot context and is recommended for hyperspectral image classification. The class-wise version should be used only when there are enough training samples.

F. Sensitivity of loss weights

In this section, we show the sensitivity of loss weights in terms of F1 score and mapping error in Figure 11, under both few-shot and many-shot settings. We do not show OA as the OA curve is similar to the F1 score. We set the classification weight from 0.1 to 0.9, and also examine two extreme cases with classification weight as 0.05 and 0.95. From the first row to the third row show results on the Pavia, Salinas, and Indian datasets, respectively. In general, both MDL4OW and MDL4OW/C can enhance the classification in terms of F1 score and mapping error, regardless of the loss weights on classification and reconstruction. One exception is Figure 11a: we can see that the class-wise method MDL4OW/C would suffer from limited training samples. MDL4OW, however, successfully improved the classification in terms of F1 score.

Although in general the methods are insensitive to the losses' weights, when under few-shot setting, a classification weight smaller than 0.2-0.3 would degrade the performance. The best results are obtained from a classification weight of 0.7-0.8. As for the many-shot setting, the performance is similar for the Pavia and Salinas data. But for the Indian data, a larger classification weight leads to a decrease on F1 score. Nevertheless, setting the classification and reconstruction weights as 0.3-0.7 can guarantee an acceptable performance of the proposed method.

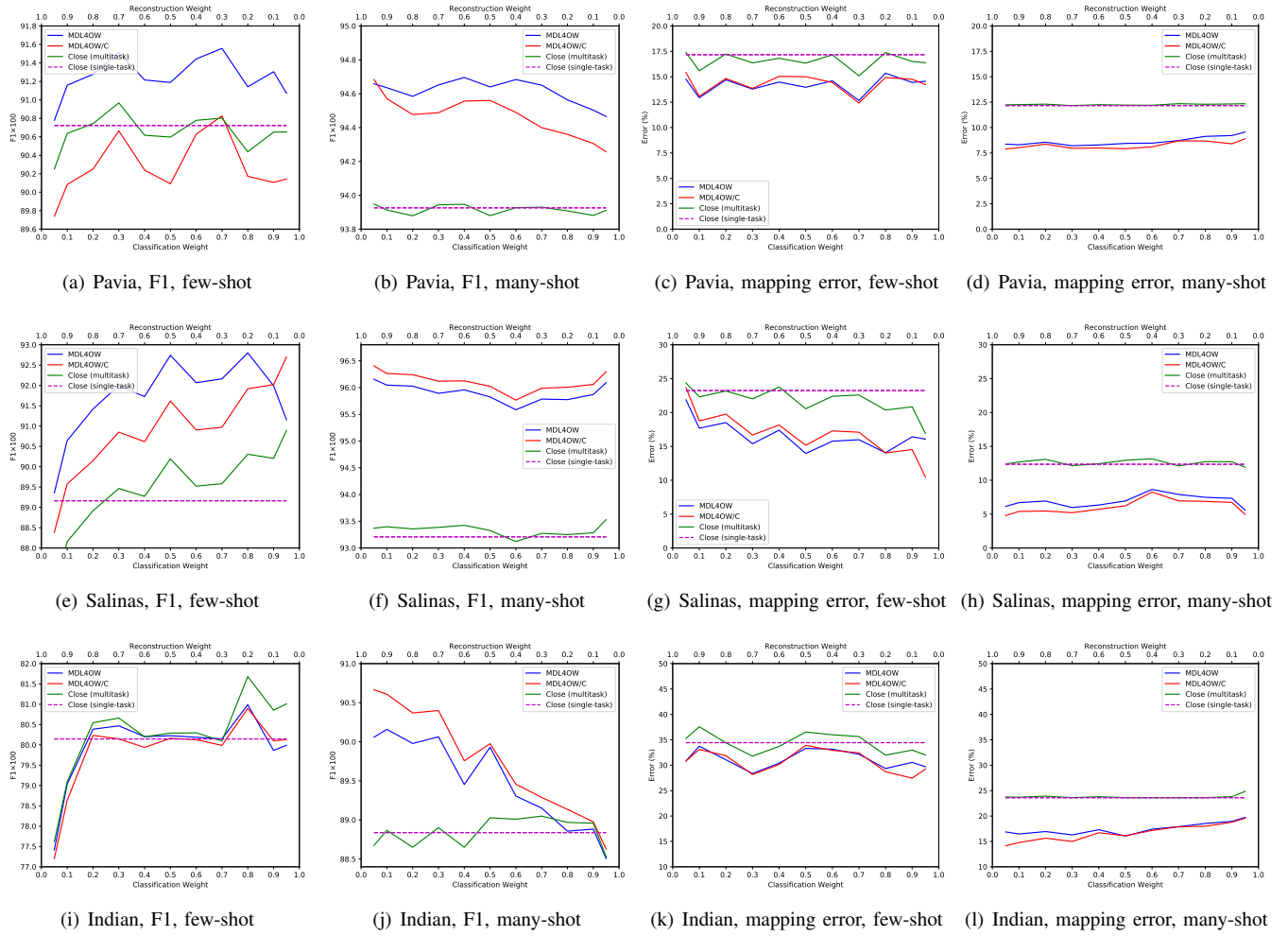


Fig. 11. Sensitivity of loss weights. From first row to the third row: results on the Pavia, Salinas, and Indian datasets, respectively. From first column to the forth column: F1 score (few-shot), F1 score (many-shot), mapping error (few-shot), mapping error (many-shot). F1 score: the larger the better; mapping error: the smaller the better.

G. Computation time

TABLE XVIII
COMPUTATION TIME IN SECONDS

	Pavia		Salinas		Indian	
	Train	Predict	Train	Predict	Train	Predict
DCCNN [29]	68	19	116	11	123	2
WCRN [73]	32	13	62	9	65	1
HResNet [43]	36	19	74	16	73	3
CROSR [52]	53	41	90	38	80	12
MDL4OW		33		30		8
MDL4OW/C	61	34	108	31	91	8

Finally, we show the computation time on the three datasets in Table XVIII under the few-shot context. Note MDL4OW and MDL4OW/C share the same training procedure and have the same training time. The training and predicting time of MDL4OW and MDL4OW/C is longer than its baseline, HResNet. This is because the added reconstruction task requires additional computation. As for CROSR, although the network used is similar with MDL4OW and MDL4OW/C, it does not compute the reconstruction error and thus has a lower training time. But, since it calculates the centroid to estimate

unknown scores, additional computation is required during the predicting phase.

V. CONCLUSIONS

In this paper, we proposed a novel multitask deep learning method for hyperspectral image classification with unknown classes in the open world, which is a first in the literature to the best of our knowledge. Conventional hyperspectral image classification assumes the classification system is complete, and there will be no unknown classes in the unseen data. This assumption is risky in the real world since the Earth's surface is complex, and it is difficult to construct a perfect classification system including all the potential classes, as shown in this study using the popular hyperspectral benchmarks as examples. In this case, the number of known classes will be overestimated, resulting in an overestimation of certain land cover, e.g., crop area for food production. To tackle this issue, a multitask deep learning method named MDL4OW is proposed for hyperspectral image classification with unknown classes, where a multitask network is utilized to simultaneously conduct classification and reconstruction. The classification provides the probability of known classes,

whereas reconstruction is used to estimate the unknown score. Extensive experiments showed that the proposed method could significantly improve the classification accuracy in terms of OA, F1, and mapping error compared with the state-of-the-art methods currently used, especially when the training samples are scarce.

Further analysis showed that the completeness of a classification system plays an important role in hyperspectral image classification with unknown classes. If a dataset is lacking basic land cover elements (impervious, vegetation, and water), the proposed method will be extremely useful to reject the unknown classes and increase the classification accuracy. However, if the classification system includes all basic land cover elements, it will be difficult to identify the unknown classes. Future works should focus on this aspect to provide more accurate hyperspectral image classification. Additionally, the use of EVT is empirical. How to properly estimate the tail distribution is essential in classification with unknown classes. Future studies may focus on this aspect and utilize Gaussian distribution, skew normal distribution, and others to obtain better classification in the open world. Code and annotations used in this paper are available at <https://sjliu.me/MDL4OW>.

ACKNOWLEDGEMENTS

The authors would like to thank Prof D. Landgrebe for making the 1992 AVIRIS Indian Pines hyperspectral data available to the community and thank Prof P. Gamba for providing the ROSIS data over Pavia, Italy, along with the reference data.

REFERENCES

- [1] R. Gebbers and V. I. Adamchuk, "Precision agriculture and food security," *Science*, vol. 327, no. 5967, pp. 828–831, 2010.
- [2] N. Audebert, B. Le Saux, and S. Lefèvre, "Semantic segmentation of earth observation data using multimodal and multi-scale deep networks," in *Asian Conference on Computer Vision*. Springer, 2016, pp. 180–196.
- [3] M. Kampffmeyer, A.-B. Salberg, and R. Jenssen, "Semantic segmentation of small objects and modeling of uncertainty in urban remote sensing images using deep convolutional neural networks," in *Proceedings of the IEEE conference on Computer Vision and Pattern Recognition Workshops*, 2016, pp. 1–9.
- [4] M. K. Ridd, "Exploring a vis (vegetation-impervious surface-soil) model for urban ecosystem analysis through remote sensing: comparative anatomy for cities," *International journal of remote sensing*, vol. 16, no. 12, pp. 2165–2185, 1995.
- [5] S. Phinn, M. Stanford, P. Scarth, A. Murray, and P. Shyy, "Monitoring the composition of urban environments based on the vegetation-impervious surface-soil (vis) model by subpixel analysis techniques," *International Journal of Remote Sensing*, vol. 23, no. 20, pp. 4131–4153, 2002.
- [6] F. Yuan, M. E. Bauer, N. J. Heinert, and G. R. Holden, "Multi-level land cover mapping of the twin cities (minnesota) metropolitan area with multi-seasonal landsat tm/etm+ data," *Geocarto International*, vol. 20, no. 2, pp. 5–13, 2005.
- [7] M. Fauvel, Y. Tarabalka, J. A. Benediktsson, J. Chanussot, and J. C. Tilton, "Advances in spectral-spatial classification of hyperspectral images," *Proceedings of the IEEE*, vol. 101, no. 3, pp. 652–675, 2012.
- [8] J. M. Bioucas-Dias, A. Plaza, G. Camps-Valls, P. Scheunders, N. Nasrabadi, and J. Chanussot, "Hyperspectral remote sensing data analysis and future challenges," *IEEE Geoscience and remote sensing magazine*, vol. 1, no. 2, pp. 6–36, 2013.
- [9] N. Audebert, B. Le Saux, and S. Lefèvre, "Deep learning for classification of hyperspectral data: A comparative review," *IEEE Geoscience and Remote Sensing Magazine*, vol. 7, no. 2, pp. 159–173, 2019.
- [10] J. A. Gualtieri and R. F. Crompt, "Support vector machines for hyperspectral remote sensing classification," in *27th AIPR Workshop: Advances in Computer-Assisted Recognition*, vol. 3584. International Society for Optics and Photonics, 1999, pp. 221–232.
- [11] B. Demir and S. Erturk, "Hyperspectral image classification using relevance vector machines," *IEEE Geoscience and Remote Sensing Letters*, vol. 4, no. 4, pp. 586–590, 2007.
- [12] P. Ghamisi, J. Plaza, Y. Chen, J. Li, and A. J. Plaza, "Advanced spectral classifiers for hyperspectral images: A review," *IEEE Geoscience and Remote Sensing Magazine*, vol. 5, no. 1, pp. 8–32, 2017.
- [13] J. Li, J. M. Bioucas-Dias, and A. Plaza, "Spectral-spatial hyperspectral image segmentation using subspace multinomial logistic regression and markov random fields," *IEEE Transactions on Geoscience and Remote Sensing*, vol. 50, no. 3, pp. 809–823, 2011.
- [14] J. A. Benediktsson, J. A. Palmason, and J. R. Sveinsson, "Classification of hyperspectral data from urban areas based on extended morphological profiles," *IEEE Transactions on Geoscience and Remote Sensing*, vol. 43, no. 3, pp. 480–491, 2005.
- [15] X. Kang, S. Li, and J. A. Benediktsson, "Spectral-spatial hyperspectral image classification with edge-preserving filtering," *IEEE transactions on geoscience and remote sensing*, vol. 52, no. 5, pp. 2666–2677, 2013.
- [16] L. Shen and S. Jia, "Three-dimensional gabor wavelets for pixel-based hyperspectral imagery classification," *IEEE Transactions on Geoscience and Remote Sensing*, vol. 49, no. 12, pp. 5039–5046, 2011.
- [17] S. Rajan, J. Ghosh, and M. M. Crawford, "An active learning approach to hyperspectral data classification," *IEEE Transactions on Geoscience and Remote Sensing*, vol. 46, no. 4, pp. 1231–1242, 2008.
- [18] Q. Shi, B. Du, and L. Zhang, "Spatial coherence-based batch-mode active learning for remote sensing image classification," *IEEE Transactions on Image Processing*, vol. 24, no. 7, pp. 2037–2050, 2015.
- [19] Q. Shi, L. Zhang, and B. Du, "Semisupervised discriminative locally enhanced alignment for hyperspectral image classification," *IEEE Transactions on Geoscience and Remote Sensing*, vol. 51, no. 9, pp. 4800–4815, 2013.
- [20] Z. Wang, B. Du, L. Zhang, L. Zhang, and X. Jia, "A novel semisupervised active-learning algorithm for hyperspectral image classification," *IEEE Transactions on Geoscience and Remote Sensing*, vol. 55, no. 6, pp. 3071–3083, 2017.
- [21] P. Ghamisi, J. A. Benediktsson, and M. O. Ulfarsson, "Spectral-spatial classification of hyperspectral images based on hidden markov random fields," *IEEE Transactions on Geoscience and Remote Sensing*, vol. 52, no. 5, pp. 2565–2574, 2013.
- [22] H. Zhang, J. Li, Y. Huang, and L. Zhang, "A nonlocal weighted joint sparse representation classification method for hyperspectral imagery," *IEEE Journal of Selected Topics in Applied Earth Observations and Remote Sensing*, vol. 7, no. 6, pp. 2056–2065, 2013.
- [23] Q. Wang, X. He, and X. Li, "Locality and structure regularized low rank representation for hyperspectral image classification," *IEEE Transactions on Geoscience and Remote Sensing*, vol. 57, no. 2, pp. 911–923, 2018.
- [24] Q. Shi, B. Du, and L. Zhang, "Domain adaptation for remote sensing image classification: A low-rank reconstruction and instance weighting label propagation inspired algorithm," *IEEE Transactions on Geoscience and Remote Sensing*, vol. 53, no. 10, pp. 5677–5689, 2015.
- [25] Q. Wang, J. Lin, and Y. Yuan, "Salient band selection for hyperspectral image classification via manifold ranking," *IEEE transactions on neural networks and learning systems*, vol. 27, no. 6, pp. 1279–1289, 2016.
- [26] C. Yu, Y. Wang, M. Song, and C.-I. Chang, "Class signature-constrained background-suppressed approach to band selection for classification of hyperspectral images," *IEEE Transactions on Geoscience and Remote Sensing*, vol. 57, no. 1, pp. 14–31, 2018.
- [27] F. Luo, L. Zhang, B. Du, and L. Zhang, "Dimensionality reduction with enhanced hybrid-graph discriminant learning for hyperspectral image classification," *IEEE Transactions on Geoscience and Remote Sensing*, 2020.
- [28] X. Lu, X. Zheng, and Y. Yuan, "Remote sensing scene classification by unsupervised representation learning," *IEEE Transactions on Geoscience and Remote Sensing*, vol. 55, no. 9, pp. 5148–5157, 2017.
- [29] H. Lee and H. Kwon, "Going deeper with contextual cnn for hyperspectral image classification," *IEEE Transactions on Image Processing*, vol. 26, no. 10, pp. 4843–4855, 2017.
- [30] L. Mou, P. Ghamisi, and X. X. Zhu, "Deep recurrent neural networks for hyperspectral image classification," *IEEE Transactions on Geoscience and Remote Sensing*, vol. 55, no. 7, pp. 3639–3655, 2017.
- [31] M. Paoletti, J. Haut, J. Plaza, and A. Plaza, "A new deep convolutional neural network for fast hyperspectral image classification," *ISPRS journal of photogrammetry and remote sensing*, vol. 145, pp. 120–147, 2018.

- [32] R. Hang, Q. Liu, D. Hong, and P. Ghamisi, "Cascaded recurrent neural networks for hyperspectral image classification," *IEEE Transactions on Geoscience and Remote Sensing*, vol. 57, no. 8, pp. 5384–5394, 2019.
- [33] S. Wan, C. Gong, P. Zhong, B. Du, L. Zhang, and J. Yang, "Multiscale dynamic graph convolutional network for hyperspectral image classification," *IEEE Transactions on Geoscience and Remote Sensing*, 2019.
- [34] S. Liu and Q. Shi, "Local climate zone mapping as remote sensing scene classification using deep learning: A case study of metropolitan china," *ISPRS Journal of Photogrammetry and Remote Sensing*, vol. 164, pp. 229–242, 2020.
- [35] Z. Zhong, J. Li, Z. Luo, and M. Chapman, "Spectral–spatial residual network for hyperspectral image classification: A 3-d deep learning framework," *IEEE Transactions on Geoscience and Remote Sensing*, vol. 56, no. 2, pp. 847–858, 2017.
- [36] B. Liu, X. Yu, A. Yu, P. Zhang, G. Wan, and R. Wang, "Deep few-shot learning for hyperspectral image classification," *IEEE Transactions on Geoscience and Remote Sensing*, vol. 57, no. 4, pp. 2290–2304, 2018.
- [37] M. Rao, P. Tang, and Z. Zhang, "Spatial–spectral relation network for hyperspectral image classification with limited training samples," *IEEE Journal of Selected Topics in Applied Earth Observations and Remote Sensing*, vol. 12, no. 12, pp. 5086–5100, 2019.
- [38] K. Gao, B. Liu, X. Yu, J. Qin, P. Zhang, and X. Tan, "Deep relation network for hyperspectral image few-shot classification," *Remote Sensing*, vol. 12, no. 6, p. 923, 2020.
- [39] Y. Zhou, J. Luo, L. Feng, and X. Zhou, "Den-based spatial features for improving parcel-based crop classification using high-resolution optical images and multi-temporal sar data," *Remote Sensing*, vol. 11, no. 13, p. 1619, 2019.
- [40] M. Golipour, H. Ghassemian, and F. Mirzapour, "Integrating hierarchical segmentation maps with mrf prior for classification of hyperspectral images in a bayesian framework," *IEEE Transactions on Geoscience and Remote Sensing*, vol. 54, no. 2, pp. 805–816, 2015.
- [41] M. Khodadadzadeh, J. Li, A. Plaza, and J. M. Bioucas-Dias, "A subspace-based multinomial logistic regression for hyperspectral image classification," *IEEE Geoscience and Remote Sensing Letters*, vol. 11, no. 12, pp. 2105–2109, 2014.
- [42] K. Makantasis, K. Karantzas, A. Doulamis, and N. Doulamis, "Deep supervised learning for hyperspectral data classification through convolutional neural networks," in *2015 IEEE International Geoscience and Remote Sensing Symposium (IGARSS)*. IEEE, 2015, pp. 4959–4962.
- [43] S. Liu and Q. Shi, "Multitask deep learning with spectral knowledge for hyperspectral image classification," *IEEE Geoscience and Remote Sensing Letters*, pp. 1–5, 2020.
- [44] N. Jamshidpour, A. Safari, and S. Homayouni, "A ga-based multi-view, multi-learner active learning framework for hyperspectral image classification," *Remote Sensing*, vol. 12, no. 2, p. 297, 2020.
- [45] Q. Liu, Z. Wu, L. Sun, Y. Xu, L. Du, and Z. Wei, "Kernel low-rank representation based on local similarity for hyperspectral image classification," *IEEE Journal of Selected Topics in Applied Earth Observations and Remote Sensing*, vol. 12, no. 6, pp. 1920–1932, 2019.
- [46] W. J. Scheirer, A. de Rezende Rocha, A. Sapkota, and T. E. Boult, "Toward open set recognition," *IEEE transactions on pattern analysis and machine intelligence*, vol. 35, no. 7, pp. 1757–1772, 2012.
- [47] A. Bendale and T. Boult, "Towards open world recognition," in *Proceedings of the IEEE conference on computer vision and pattern recognition*, 2015, pp. 1893–1902.
- [48] D. Tuia, E. Pasolli, and W. J. Emery, "Using active learning to adapt remote sensing image classifiers," *Remote Sensing of Environment*, vol. 115, no. 9, pp. 2232–2242, 2011.
- [49] A. Bendale and T. E. Boult, "Towards open set deep networks," in *Proceedings of the IEEE conference on Computer Vision and Pattern Recognition*, 2016, pp. 1563–1572.
- [50] L. Neal, M. Olson, X. Fern, W.-K. Wong, and F. Li, "Open set learning with counterfactual images," in *Proceedings of the European Conference on Computer Vision (ECCV)*, 2018, pp. 613–628.
- [51] A. R. Dhamija, M. Günther, and T. Boult, "Reducing network agnostophobia," in *Advances in Neural Information Processing Systems*, 2018, pp. 9157–9168.
- [52] R. Yoshihashi, W. Shao, R. Kawakami, S. You, M. Iida, and T. Nae-mura, "Classification-reconstruction learning for open-set recognition," in *Proceedings of the IEEE Conference on Computer Vision and Pattern Recognition*, 2019, pp. 4016–4025.
- [53] A. Krizhevsky, V. Nair, and G. Hinton, "Cifar-10 and cifar-100 datasets," URL: <https://www.cs.toronto.edu/kriz/cifar.html>, vol. 6, 2009.
- [54] H. Xiao, K. Rasul, and R. Vollgraf, "Fashion-mnist: a novel image dataset for benchmarking machine learning algorithms," *arXiv preprint arXiv:1708.07747*, 2017.
- [55] B. Pan, Z. Shi, and X. Xu, "Mugnet: Deep learning for hyperspectral image classification using limited samples," *ISPRS Journal of Photogrammetry and Remote Sensing*, vol. 145, pp. 108–119, 2018.
- [56] S. Xu, J. Li, M. Khodadadzadeh, A. Marinoni, P. Gamba, and B. Li, "Abundance-indicated subspace for hyperspectral classification with limited training samples," *IEEE Journal of Selected Topics in Applied Earth Observations and Remote Sensing*, vol. 12, no. 4, pp. 1265–1278, 2019.
- [57] J. Deng, W. Dong, R. Socher, L.-J. Li, K. Li, and L. Fei-Fei, "Imagenet: A large-scale hierarchical image database," in *2009 IEEE conference on computer vision and pattern recognition*. Ieee, 2009, pp. 248–255.
- [58] C. Geng and S. Chen, "Collective decision for open set recognition," *IEEE Transactions on Knowledge and Data Engineering*, 2020.
- [59] K. He, X. Zhang, S. Ren, and J. Sun, "Deep residual learning for image recognition," in *Proceedings of the IEEE conference on Computer Vision and Pattern Recognition*, 2016, pp. 770–778.
- [60] M. Lin, Q. Chen, and S. Yan, "Network in network," *arXiv preprint arXiv:1312.4400*, 2013.
- [61] J. Pan, E. Sayrol, X. Giro-i Nieto, K. McGuinness, and N. E. O'Connor, "Shallow and deep convolutional networks for saliency prediction," in *Proceedings of the IEEE Conference on Computer Vision and Pattern Recognition*, 2016, pp. 598–606.
- [62] L. Zhang, L. Zhang, and B. Du, "Deep learning for remote sensing data: A technical tutorial on the state of the art," *IEEE Geoscience and Remote Sensing Magazine*, vol. 4, no. 2, pp. 22–40, 2016.
- [63] S. Ioffe and C. Szegedy, "Batch normalization: Accelerating deep network training by reducing internal covariate shift," *arXiv preprint arXiv:1502.03167*, 2015.
- [64] V. Nair and G. E. Hinton, "Rectified linear units improve restricted boltzmann machines," in *Proceedings of the 27th international conference on machine learning (ICML-10)*, 2010, pp. 807–814.
- [65] J. Pickands III *et al.*, "Statistical inference using extreme order statistics," *the Annals of Statistics*, vol. 3, no. 1, pp. 119–131, 1975.
- [66] S. D. Grimshaw, "Computing maximum likelihood estimates for the generalized pareto distribution," *Technometrics*, vol. 35, no. 2, pp. 185–191, 1993.
- [67] P. Oza and V. M. Patel, "C2ae: Class conditioned auto-encoder for open-set recognition," in *Proceedings of the IEEE Conference on Computer Vision and Pattern Recognition*, 2019, pp. 2307–2316.
- [68] C. Geng, S.-j. Huang, and S. Chen, "Recent advances in open set recognition: A survey," *IEEE Transactions on Pattern Analysis and Machine Intelligence*, 2020.
- [69] Z. Liu, Z. Miao, X. Zhan, J. Wang, B. Gong, and S. X. Yu, "Large-scale long-tailed recognition in an open world," in *Proceedings of the IEEE Conference on Computer Vision and Pattern Recognition*, 2019, pp. 2537–2546.
- [70] M. Abadi, P. Barham, J. Chen, Z. Chen, A. Davis, J. Dean, M. Devin, S. Ghemawat, G. Irving, M. Isard *et al.*, "Tensorflow: A system for large-scale machine learning," in *12th {USENIX} Symposium on Operating Systems Design and Implementation ({OSDI} 16)*, 2016, pp. 265–283.
- [71] F. Chollet *et al.*, "Keras," <https://github.com/fchollet/keras>, 2015.
- [72] M. D. Zeiler, "Adadelata: an adaptive learning rate method," *arXiv preprint arXiv:1212.5701*, 2012.
- [73] S. Liu, H. Luo, Y. Tu, Z. He, and J. Li, "Wide contextual residual network with active learning for remote sensing image classification," in *IGARSS 2018-2018 IEEE International Geoscience and Remote Sensing Symposium*. IEEE, 2018, pp. 7145–7148.
- [74] W. Hu, Y. Huang, L. Wei, F. Zhang, and H. Li, "Deep convolutional neural networks for hyperspectral image classification," *Journal of Sensors*, vol. 2015, 2015.
- [75] W. Li, G. Wu, F. Zhang, and Q. Du, "Hyperspectral image classification using deep pixel-pair features," *IEEE Transactions on Geoscience and Remote Sensing*, vol. 55, no. 2, pp. 844–853, 2016.
- [76] S. Mei, J. Ji, J. Hou, X. Li, and Q. Du, "Learning sensor-specific spatial-spectral features of hyperspectral images via convolutional neural networks," *IEEE Transactions on Geoscience and Remote Sensing*, vol. 55, no. 8, pp. 4520–4533, 2017.
- [77] X. Lu, W. Zhang, and X. Li, "A hybrid sparsity and distance-based discrimination detector for hyperspectral images," *IEEE Transactions on Geoscience and Remote Sensing*, vol. 56, no. 3, pp. 1704–1717, 2017.